

Near-Oracle KV Selection via Pre-hoc Sparsity for Long-Context Inference

Yifei Gao[†], Lei Wang[†], *Senior Member, IEEE*, Rong-Cheng Tu[†], Qixin Zhang,
Jun Cheng^{*}, *Senior Member, IEEE*, and Dacheng Tao, *Fellow, IEEE*

Abstract—A core bottleneck in large language model (LLM) inference is the cost of attending over the ever-growing key–value (KV) cache. Although near-oracle top- k KV selection can preserve the quality of dense attention while sharply reducing computation and bandwidth, existing sparse methods generally rely on posterior heuristics—selectors conditioned on observed attention or proxy scores. Such conditioning introduces posterior bias: it tends to distort the true token importance and miss salient tokens, thereby impairing long-range reasoning. To tackle this problem, we propose Pre-hoc Sparsity (PrHS), which selects KV entries before attention scoring and provides explicit accuracy control. Let the attention mass of discarded entries be δ (the dropped mass). Through a marginal-to-mutual-information analysis, we derive an upper bound on the mutual-information loss that depends only on δ . This relation both explains the failure modes of posterior heuristics and enables verifiable guarantees by controlling δ in advance. Within PrHS, we instantiate three orthogonal pre-hoc selectors along the axes of time, depth, and layer: (i) temporal query sharing, justified by a Lipschitz bound on attention-centroid drift so that a modest dilation of the previously shared set covers the next step; (ii) recency-window retention, leveraging distance-decay priors to guarantee retained attention mass; and (iii) cross-layer KV sharing, exploiting high inter-layer similarity to eliminate redundant retrieval and computation. Extensive experiments on LLaMA and Mistral families validate the superiority of PrHS. On LLaMA and Mistral families across GSM8K and CoQA, the approach reduces retrieval overhead by >90%, achieving $3\times$ higher retrieval sparsity than the state-of-the-art HShare at matched or better accuracy. It also incurs <1% average degradation on LongBench, lowers attention FLOPs by $\sim 15\%$ versus prior sparse baselines, and yields a $9.9\times$ speedup in attention-operator latency and $2.8\times$ higher throughput on NVIDIA A100-80GB GPUs than the original dense baseline.

I. INTRODUCTION

LARGE Language Models (LLMs) [1, 2, 3] empower advanced applications such as multi-turn dialogue [4, 5, 6], long-form document summarization [7, 8], and multimodal

This work was supported in part by the Guangdong Major Project of Basic and Applied Basic Research (2023B0303000016), Guangdong S&T Program (No. 2024B0101050002), Guangdong-Hong Kong-Macao Joint Laboratory of Human-Machine Intelligence-Synergy Systems (2019B121205007), CAS Key Technology Talent Program, Colleges and Universities Key Laboratory of Intelligent Integrated Automation (No.201502), CAS Key Laboratory of Human-Machine Intelligence-Synergy Systems, Shenzhen Institutes of Advanced Technology, Chinese Academy of Sciences (2014DP173025).

Manuscript received July 1, 2025; revised XX, 2025. (Corresponding author: jun.cheng@siat.ac.cn)

Yifei Gao is with University College London, London, UK. (E-mail: ucabaoj@ucl.ac.uk).

Lei Wang and Jun Cheng are with the Shenzhen Institutes of Advanced Technology, Chinese Academy of Sciences (CAS), Shenzhen 518055, China. They are also with the Chinese University of Hong Kong. (e-mail: lei.wang1@siat.ac.cn, jun.cheng@siat.ac.cn).

Rong-Cheng Tu, Qixin Zhang and Dacheng Tao are with the College of Computing & Data Science, Nanyang Technological University, Singapore. (E-mail: rongcheng.tu@ntu.edu.sg, qixin.zhang@ntu.edu.sg, dacheng.tao@ntu.edu.sg)

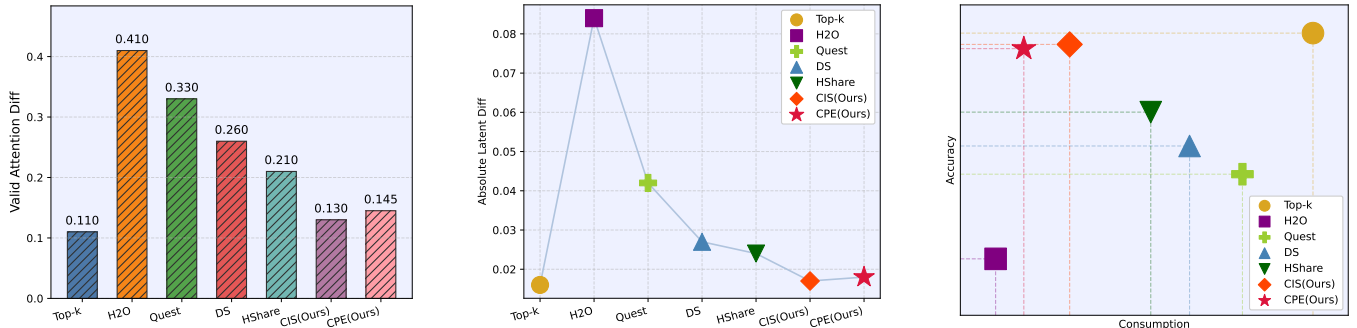
tasks [9, 10, 11, 12, 13, 14] involving text and visual understanding [15, 16, 17, 18, 19, 20]. However, in autoregressive decoding, the per-layer key–value (KV) cache grows linearly with the generated length L , requiring each new query to access an increasingly large set of past KVs. With H heads and per-head dimension d , the per-query attention cost (score computation and value aggregation) scales as $\mathcal{O}(HLd)$ [21]. As L increases, runtime becomes dominated by attention computation rather than model forward passes; for example, at a 40k-token context, LLaMA-3.1-8B [22] incurs attention compute on the order of tens of TFLOPs per decoding step.

KV compression alleviates these costs by exploiting attention sparsity [23, 24, 25, 26]: most KV entries receive negligible attention, so retaining a small, critical subset can approximate full attention while reducing memory traffic and latency. With a per-head budget $k \ll L$, the top- k oracle retains the k highest-score entries per query, minimizing approximation error and achieving the best accuracy. While this reduces value aggregation from $\mathcal{O}(HLd)$ to $\mathcal{O}(Hkd)$, identifying the top- k still requires computing all scores at $\mathcal{O}(HLd)$ plus a retrieval overhead. Thus, end-to-end cost remains dominated by full scoring, making the oracle impractical for deployment.

To simplify full scoring, existing approaches approximate the top- k oracle by summarizing observed (posterior) attention statistics into priors that constrain future retrieval, yielding posterior-conditioned policies. For example, *Token Dropping Oracles* (TDOs) apply static or dynamic eviction policies [25, 26, 27, 28] to keep only entries deemed critical at the current step, restricting the candidate set and reducing per-step scoring to $\mathcal{O}(Hkd)$. *Query-Aware Approximations* (QAAs) [29, 30, 31, 32] construct low-dimensional, hand-designed surrogate features to approximate attention scores and use them to guide retrieval, incurring $\mathcal{O}(HLd')$ with $d' \ll d$.

Despite the efficiency gains, these posterior-driven simplifications incur systematic bias that degrade generative performance. Specifically, in TDO, token salience evolves over time. Thus, selectors that condition on observed attention along the trajectory face non-stationary evidence and systematically skew future decisions [28, 30]. In addition, QAAs that replace full logits with heuristic proxies induce a score-level bias. We group these archetypes under **Post-hoc Sparsity (PoHS)**—*posterior-conditioned* rules that bias token-importance estimates and thereby impair long-range reasoning. Empirically, PoHS yields substantially larger perturbations at both the attention and the output (latent) levels than the top- k oracle (Fig. 1a, 1b; lower is better).

Therefore, in this paper, we analyze selection through a *marginal-to-mutual-information* lens and devise a new



(a) Introduced attention disturbances (absolute difference) after filtering pre-softmax attention logits < 0.

(b) Introduced absolute differences between original attention outputs.

(c) Overall comparisons on accuracy-consumption trade-offs among state-of-the-art baselines.

Fig. 1. **Overall analysis of performance and efficiency.** Across induced attention-approximation error and accuracy-efficiency trade-offs, our method consistently surpasses prior SOTA approaches and closely tracks the top- k oracle for optimal KV compression accuracy.

framework, **Pre-hoc Sparsity** (PrHS). Let δ denote the dropped attention mass (mass of discarded KV entries), and let ΔH quantify the induced perturbation of the attention distribution. We prove that the selection-induced *mutual-information loss* admits an upper bound that depends only on δ (Eq. (9)). This provides an a-priori error certificate: by constraining δ before scoring, PrHS instantiates selectors that avoid posterior bias and delivers explicit selection-error control by enforcing conditions that tighten the bound. Consequently, PrHS markedly reduces attention- and output-level perturbations and approaches the oracle frontier in the accuracy-efficiency trade-off (Fig. 1c). We further quantify deviation from the oracle by β_{th} , the marginal-entropy gap between PrHS and top- k ; as $\beta_{\text{th}} \rightarrow 0$, PrHS converges to the oracle (Eq. 10; proof in Sec. VIII).

We instantiate three PrHS techniques, Clustered Index Sharing (CIS), Progressive Sliding Attention Window (PSAW), and Early Token Freezing (ETF), each translating a distinct sparsity prior into a PrHS selector. These selectors are then parameterized to tighten the MI upper bound on marginal-entropy error (Eq. (9)). CIS explores temporal-locality [33]: consecutive queries are highly similar. It shares the retrieved set from the top- k oracle across temporally adjacent queries whose embeddings exceed a cosine-similarity threshold, and dilates it by adding neighbors around highest-score indices. PSAW leverages the recency prior [26, 25]—attention mass concentrates on a local window—and applies a depth-adaptive sliding window that shrinks monotonically with depth, incrementally pruning the candidate KV entries. ETF exploits cross-layer redundancy [34]: adjacent layers exhibit high KV similarity. ETF freezes stable early tokens to reduce updates. The three selectors act along different axes—time (CIS), depth (PSAW), and layer (ETF)—and compose naturally: CIS seeds the candidate pool with a small budget, then PSAW and ETF intersect their selections with the CIS seed using larger budgets to further prune. Finally, we implement custom CUDA kernels that parallelize index manipulation and sparse-attention computation to minimize runtime overhead. We refer to the combined system as **CPE**.

Collectively, CPE delivers competitive reductions in memory footprint and end-to-end latency with substantially improved relative to state-of-the-art (SOTA) baselines (Fig. 1c). Empirically, on LLaMA [22] and Mistral model families [35]

across GSM8K and CoQA, CIS matches the accuracy of recent SOTA method HShare [33] while using only *one-third* of its retrieval complexity. Overall, CPE maintains comparable model quality even with reducing > 90% KV-retrieval overhead, while lowering $\sim 15\%$ attention FLOPs than prior sparse baselines. On NVIDIA A800-80GB GPUs, CPE attains a **9.9 \times** speedup in attention-operator latency and a **2.8 \times** throughput improvement over original models. Ablation studies in Sec. V-E2 further confirm that each component contributes reliably. Our contributions are summarized as follows:

- 1) Rigorous analyses of the mutual information bound from the marginal entropy in KV compression and introduction of Pre-hoc Sparsity towards the accuracy of top- k oracle.
- 2) Introduction of CIS, which sustains stable performance at high sharing ratios, together with PSAW and ETF for lossless sparsification of attention computation, all implemented with customized CUDA kernels for parallelization.
- 3) Extensive experiments and ablations demonstrating consistent improvements in accuracy, efficiency, and throughput over state-of-the-art baselines.

II. PROBLEM FORMULATION

This section introduces several variables and notation used throughout our analysis. For convenience, Table I summarizes the key symbols and their meanings.

A. LLM Inference

To demonstrate the inference bottlenecks that KV compression aims to address, we present the inference process, consisting of two stages—prefill and decode—using the standard transformer architecture with multi-head attention [21].

a) *Multi-head Attention*: Let the input token embeddings for head h be $\mathbf{x}^h = [\mathbf{x}_1^h; \dots; \mathbf{x}_L^h] \in \mathbb{R}^{L \times d}$. With H heads and per-head dimension d , for each token i and head $h \in 1, \dots, H$,

$$\mathbf{q}_i^h = \mathbf{x}_i \mathbf{W}_Q^h, \mathbf{k}_i^h = \mathbf{x}_i \mathbf{W}_K^h, \mathbf{v}_i^h = \mathbf{x}_i \mathbf{W}_V^h, \quad (1)$$

where $\mathbf{q}_i^h, \mathbf{k}_i^h, \mathbf{v}_i^h \in \mathbb{R}^d$ and $\mathbf{K}^h = [(\mathbf{k}_1^h)^\top; \dots; (\mathbf{k}_L^h)^\top]$, $\mathbf{V}^h = [(\mathbf{v}_1^h)^\top; \dots; (\mathbf{v}_L^h)^\top] \in \mathbb{R}^{L \times d}$ to form the KV cache. Attention

TABLE I
SUMMARY OF KEY VARIABLES AND NOTATION.

\mathbf{x}	Input token embedding	$\mathbf{q}, \mathbf{k}, \mathbf{v}$	Query, key, value
L	Input length	d	Per-head dimension
H	Number of heads	$A(\cdot)$	Attention weight
\mathbf{K}, \mathbf{V}	KV cache matrices	t	Step count
S	Selector returning a subset of indices	S_t	Selected KV index set at step t
N	KV budget (sparsity: N/t)	$\tau(\cdot)$	Retained attention mass
$\delta(\cdot)$	Dropped attention mass	I_{full}, I_S	MI under full attention vs. TSA
$g(\cdot)$	MI-loss bound function	$\delta^*(\cdot)$	Oracle (top- k) dropped mass

weights for token t in head h over indices $i \in 1, \dots, t$ and the attention output for step t are

$$A_i^h(\mathbf{q}_t^h) = \frac{\exp((\mathbf{q}_t^h)^\top \mathbf{k}_i^h / \sqrt{d})}{\sum_{j=1}^t \exp((\mathbf{q}_t^h)^\top \mathbf{k}_j^h / \sqrt{d})}, \quad \mathbf{y}_t^h = \sum_{i=1}^t A_i^h(\mathbf{q}_t^h) \mathbf{v}_i^h. \quad (2)$$

Since all heads operate the same, we omit the head index for brevity in the following context, unless explicitly mentioned.

b) Prefill: The prompt is processed once to construct and cache (\mathbf{K}, \mathbf{V}) , which is reused during subsequent decoding [36].

c) Decode: Only the new token is processed while reusing the cached \mathbf{K} and \mathbf{V} from previous steps for each head.

d) Bottlenecks: From Eq. (2), the per-step attention FLOPs (score computation and value aggregation) scale as $\mathcal{O}(Htd)$, and the KV cache also scales as $\mathcal{O}(Htd)$. This linear growth in t constitutes the primary compute and memory bottleneck for long-context inference.

B. Token-sparse Attention and Key-value Sharing

KV compression mitigates the aforementioned bottlenecks by exploiting attention sparsity—a small subset of critical KV entries is selected to approximate full attention. This improves efficiency at the cost of approximation error. To evaluate accuracy–efficiency trade-offs across KV compression methods, and following prior work [37, 31, 33, 38], we formalize decoding with a limited KV set under a unified *token-sparse attention* (TSA) concept, and then define *KV sharing* as a special case that streamlines TSA selection.

Definition 3.1 (Token-sparse attention, informal). *At decoding step t , with KV budget $N < t$, a selector S outputs an index set $S_t \subseteq [t] := \{1, \dots, t\}$ with $|S_t| = N$. The corresponding key/value matrices are restricted to these indices, \mathbf{K}_{S_t} and \mathbf{V}_{S_t} . Attention is computed only between \mathbf{q}_t and \mathbf{K}_{S_t} (cf. Eq. (2)), and the output uses \mathbf{V}_{S_t} . The sparsity ratio at step t is N/t .*

Definition 3.2 (Key-value sharing). *Given indices S_i retrieved by S at an anchor step i in TSA, a later token at step j may directly reuse them, denoted $S_j \leftarrow S_i$. In this case, S_j is utilized to construct \mathbf{K}_{S_j} and \mathbf{V}_{S_j} .*

Discussion. Different TSA instantiations correspond to different selectors S , and exhibit distinct accuracy–efficiency trade-offs under a fixed budget. For example, imprecise selection that admits many low-contribution pairs can crowd out salient

entries, increasing approximation error and degrading model performance. This failure mode is analogous to erroneous KV sharing across steps whose truly critical sets have little overlap. Moreover, selectors rely on different criteria [32, 25, 30] (e.g., similarity heuristics, learned scores, recency rules), and the mechanism used to enforce these criteria determines selection complexity and entry-retrieval efficiency. Consequently, an effective TSA selector must balance accuracy (retained mass) and retrieval overhead (selection complexity).

C. Information Loss Quantification

To evaluate the accuracy of TSA selectors, we quantify the information loss—information gap between full attention and TSA—via a mutual-information (MI) bound, and pair it with retrieval-efficiency analysis to guide algorithm design. We first derive the MI bound as a function of dropped attention mass, which implies that the top- k oracle attains the best accuracy under a fixed budget. However, it incurs prohibitive selection cost due to explicit attention evaluation. Practical selectors approximate this oracle for efficiency and thus incur additional MI loss. We then formalize selector design as an optimization problem towards minimizing the MI-loss gap relative to the top- k oracle subject to retrieval constraints. Finally, we show that PrHS-based selectors remove posterior bias and, with design-time error control, nearly preserve top- k accuracy without additional retrieval cost, thereby outperforming PoHS selectors.

a) Mutual-information Bound: In TSA, a selector S keeps N KV entries and drops the rest. Our core result (Sec. VII) is that the MI loss induced by TSA depends only on the *dropped mass*, independent of selector instantiations. Intuitively, preserving (nearly) the same total attention mass as full attention preserves (nearly) the same information. Hence, MI loss admits a unified characterization in terms of dropped mass. For a query \mathbf{q} , define the retained and dropped attention mass

$$\tau_S(\mathbf{q}) = \sum_{i \in S} A_i(\mathbf{q}), \quad \delta_S(\mathbf{q}) = 1 - \tau_S(\mathbf{q}). \quad (3)$$

Let I denote the MI loss measure. For any \mathbf{q} , the MI loss between full attention I_{full} and selector S satisfies

$$0 \leq I_{\text{full}}(\mathbf{q}) - I_S(\mathbf{q}) \leq g(\delta_S(\mathbf{q})), \quad (4)$$

where $g(\delta) := 2[h_b(\delta) + \delta \log L]$.

Here h_b is the binary entropy function and L the number of eligible positions (proved in Sec. VII-B).

b) Top- k Oracle and Optimization Goal: The top- k oracle $S^*(q) = \text{Top}_N(A(\mathbf{q}))$ minimizes the bound by maximizing retained mass under a fixed budget N :

$$S^*(\mathbf{q}) \in \underset{S \subseteq [t], |S|=N}{\operatorname{argmin}} g\left(1 - \sum_{i \in S} A_i(\mathbf{q})\right) = \underset{S \subseteq [t], |S|=N}{\operatorname{argmax}} \sum_{i \in S} A_i(\mathbf{q}). \quad (5)$$

However, evaluating $A(\mathbf{q})$ exactly incurs prohibitive selection cost. Practical selectors (PoHS or PrHS) approximate $A(\mathbf{q})$ for efficiency and thus incur additional MI loss. We therefore pose the goal of selector optimization as

$$\min \mathbb{E}[I_{S^*}(\mathbf{q}) - I_S(\mathbf{q})] \quad \text{s.t.} \quad |S^*(\mathbf{q})| = |S(\mathbf{q})| = N, \quad (6)$$

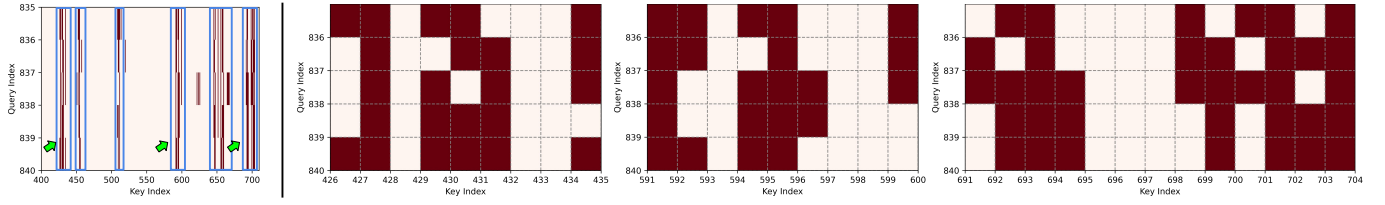


Fig. 2. **Distribution of critical indices in LLaMA2-7B-Chat (Layer 10, Head 2).** For each query, we retrieve 64 critical indices using the top- k oracle on WikiText2. Columns show five temporally adjacent queries with cosine similarity > 0.8 . *Left*: overall distribution across keys 400–710; clusters are outlined in blue boxes. *Right*: zoom-ins of three clusters (annotated by green arrows in the left) at keys 426–436, 591–700, and 691–704. Critical indices are in red.

i.e., minimize the MI-loss gap relative to the top- k oracle under constrained budget, where the expectation is over queries \mathbf{q} .

c) *PoHS Selector* \mathcal{S}_D : $\mathcal{S}_D(\mathbf{q}) = \text{Top}_n(\hat{A}_D(\mathbf{q}))$ replaces $A(\mathbf{q})$ with its surrogate $\hat{A}_D(\mathbf{q})$ derived from posterior side information D (e.g., token ages, sketches), and suffers *posterior bias* measured by the total-variation distance

$$\varepsilon_D(\mathbf{q}) := \frac{1}{2} \|A(\mathbf{q}) - \hat{A}_D(\mathbf{q})\|_1. \quad (7)$$

The extra dropped-mass gap satisfies $\delta_{\mathcal{S}_D}(\mathbf{q}) \leq \delta^*(\mathbf{q}) + 2\varepsilon_D(\mathbf{q})$, which, by the monotonicity¹ of g in Eq. (4), lifts the MI loss bound to

$$I_{\text{full}}(\mathbf{q}) - I_{\text{post}}(\mathbf{q}) \leq g(\delta^*(\mathbf{q}) + 2\varepsilon_D(\mathbf{q})). \quad (8)$$

Thus, when the surrogate under- or over-scores tokens (large ε_D), the selected set retains less probability mass than the oracle and loses more information. We formalize both TDO and QAA from Sec. I as PoHS instances. In general, TDO induces larger ε_D than QAA (worse accuracy) but avoids explicit evaluation of $A(\mathbf{q})$ (lower retrieval cost). Proofs are provided in Sec. VII-B.

d) *PrHS Selector* \mathcal{S}_{pre} : \mathcal{S}_{pre} selects critical set *without explicitly computing* $A(\mathbf{q})$ and controls a *theoretical error* $\beta_{\text{th}}(q) \geq 0$ that satisfy

$$\tau_{\text{pre}}(\mathbf{q}) \geq \tau^*(\mathbf{q}) - \beta_{\text{th}}(\mathbf{q}) \iff \delta_{\text{pre}}(\mathbf{q}) \leq \delta^*(\mathbf{q}) + \beta_{\text{th}}(\mathbf{q}), \quad (9)$$

with $I_{\text{full}}(\mathbf{q}) - I_{\text{pre}}(\mathbf{q}) \leq g(\delta^*(\mathbf{q}) + \beta_{\text{th}}(\mathbf{q}))$.

As $\beta_{\text{th}}(q) \rightarrow 0$, the bound *converges to the top- k oracle*

$$I_{\text{full}}(\mathbf{q}) - I_{\text{pre}}(\mathbf{q}) \leq g(\delta^*(\mathbf{q})) \leq g(\delta^*(\mathbf{q}) + 2\varepsilon_D(\mathbf{q})), \quad (10)$$

explicitly improving on PoHS by eliminating posterior bias. Detailed formulations are in Sec. VIII. Moreover, PrHS selectors can partially (CIS) or fully (PSAW, ETF) avoid computing $A(\mathbf{q})$ and the associated retrieval, improving accuracy without compromising efficiency.

III. OBSERVATIONS AND PROPERTIES

While empirical priors (temporal locality, recency, cross-layer redundancy) are suggestive, PrHS requires *query-independent* design rules that can be applied pre-hoc without full attention. Accordingly, from the transformer’s mechanics we derive two properties: (i) clustered locality and among-query continuity of critical indices, and (ii) progressive cross-layer propagation

¹Without loss of generality, in this paper, we restrict the domain of g to the interval $(0, L/(1+L)]$ to ensure its monotonicity, where L denotes the current text length. Note that as L grows large, $L/(1+L)$ will approach 1, which renders the previous restriction reasonable.

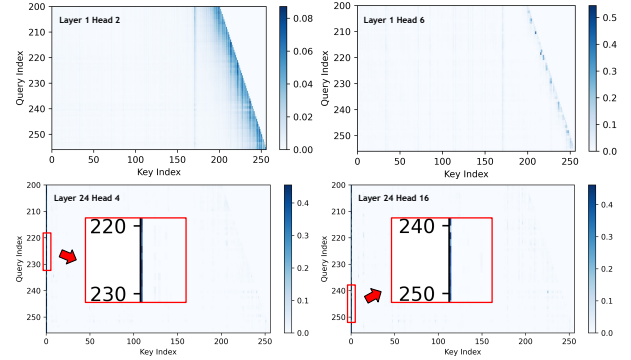


Fig. 3. **Attention distribution on LLaMA2-7B-Chat.** Heatmaps across representative layer-head pairs, with darker color indicating stronger attention.

of information. These properties motivate our selector parameterization and, in Sec IV, yield a retained-mass guarantee $\tau_{\text{pre}} \geq \tau^* - \beta_{\text{th}}$, which translates to MI bounds via Eq. (4).

A. Observation 1: Critical Tokens Exist in Clustered Manners

Prior work [30, 39, 33] shows that consecutive decoding queries are close in embedding space and often share critical indices, which motivates KV sharing strategies. However, *per-head* selections can still vary markedly, and the overlap between selected indices remains small even for high cosine similarity between queries [31], leading to suboptimal sharing. For example, HShare [33] shares indices directly, missing many truly critical indices at high sharing ratios. To bridge this gap, we observe that critical indices organize into a small number of clusters that persist across adjacent queries, providing a more stable sharing unit than individual indices.

Property 1 (Among-query Property). *For two semantically similar consecutive queries, the centroids of their critical-token clusters undergo a smooth mean shift along the sequence axis.*

As shown in Fig. 2, when the cosine similarity between q_t and q_{t+1} exceeds 0.8, critical indices concentrate into a few clusters; although cluster centers and spreads shift slightly, the cluster-level overlap remains large. Our theoretical analysis further shows that these clusters satisfy a mean-shift (bounded drift) property, formalized in **Theorem 1**.

Theorem 1 (Centroid Drift). *Consider the scaled dot-product self-attention (cf. Eq. (2)) with fixed keys $\{\mathbf{k}_j\}_{j=1}^t$, attention weights $A_j(\mathbf{q}_t)$ for key \mathbf{k}_j , and let $\{p_j\}_{j=1}^t$ be scalar token positions with $\text{diam } \mathcal{P} := \max_j p_j - \min_j p_j$ for $\mathcal{P} = \{p_j\}$.*

Define the sequence-axis centroid $c(\mathbf{q}_t) = \sum_j A_j(\mathbf{q}_t) p_j$. For $\mathbf{q}' = \mathbf{q}_t + \Delta$ with $\|\Delta\| \ll 1$,

$$c(\mathbf{q}') = c(\mathbf{q}_t) + O(\|\Delta\|), \quad (11)$$

i.e., the attention centroid moves in a Lipschitz-continuous fashion with respect to the query. In particular, $|c(\mathbf{q}') - c(\mathbf{q}_t)| \leq (\text{diam } \mathcal{P}) \frac{\max_j \|\mathbf{k}_j\|}{\sqrt{d}} \|\Delta\|$.

The drift is $\mathcal{O}(\|\Delta\|)$ with Lipschitz modulus $L \leq (\text{diam } \mathcal{P}) \max_j \|\mathbf{k}_j\| / \sqrt{d}$. This smooth drift is consistent with empirical attention patterns and with StreamingLLM’s “keep a few initial tokens” observation [26].

In summary, **across heads and layers, the critical tokens of successive similar queries form dense, localized clusters.** We call this the **sink effect**: *tokens near a high-attention location inherit elevated attention due to semantic proximity.* Exploring the effect enables explicit control under PrHS, our CIS operationalizes this by dilating shared sets to cover the local cluster and compensate for centroid drift, avoiding full per-head re-retrieval. Detailed proofs are in **Appendix A**.

B. Observation 2: Information Propagates Progressively Among Layers

Locality-bias analyses [25, 40] show that attention is sharply concentrated locally within a narrow window around the current query and the sink token, across diverse prompts (Fig. 3). This suggests that the current token draws most information from recent tokens, whereas the sink token acts as an attractor rather than conveying semantic content. Viewed in isolation, such constrained receptive fields would only support short-term memory for LLMs, seemingly at odds with their strong long-context performance. Moreover, recent studies [41, 28, 42] show that: across layers, intermediate tokens incrementally absorb the semantics of their relevant predecessors; by higher layers, a mid-sequence token encodes both its own content and a compressed synopsis of earlier, distant tokens. It means that stacking transformer layers realizes long-range dependency paths through chains of neighboring tokens even when no individual layer attends broadly. Consequently, salient long-distance information is distilled into nearby carrier tokens, reducing the marginal importance of many earlier ones; hence, later layers need not re-scan the full prefix. Building on this insight, PSAW and ETF prune KV entries whose instantaneous (per-layer) and accumulated (cross-layer) attention mass fall below preset thresholds, ensuring that the total dropped mass remains within β_{th} ; by Eq. (4), this certifies a bounded MI loss. We formalize these guarantees in **Appendix C-D**.

IV. PROPOSED METHOD AND IMPLEMENTATION

In this section we present CPE. First, **CIS** (from Observation 1) enables efficient head-level KV sharing across adjacent queries. Next, **PSAW** and **ETF** (from Observation 2) prune redundant attention by shrinking visible attention window and freezing early token updates, respectively, with theoretical error guarantees. We also describe CUDA kernels for parallel index manipulation and sparse attention.

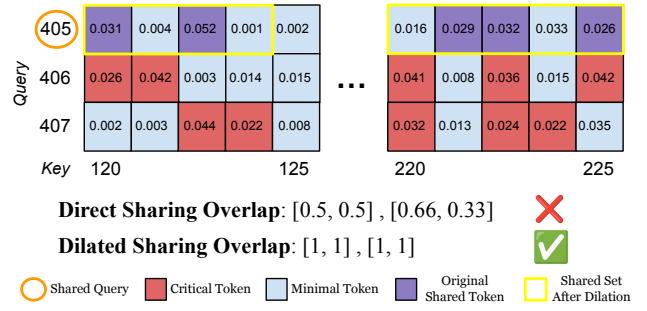


Fig. 4. **Critical-index set (CIS) dilation.** For three adjacent queries (405–407), we examine two key-index clusters [120, 125] and [220, 225]. Critical tokens from query 405 are shared to queries 406 and 407. Overlap is measured as $\frac{\text{Number of True Positive}}{\text{Number of Critical Tokens}}$. Tokens in violet are also critical for query 405.

A. Clustered Indices Sharing (CIS)

CIS performs head-level KV sharing with dilated shared set among semantically similar, and temporally adjacent queries. By **Observation 1** and **Theorem 1**, the critical clusters for such queries undergo only small mean shifts relative to a reference query. Therefore, exhaustive per-query head-level retrieval is unnecessary. We first partition the sequence into fixed-length blocks and restrict sharing to within a block to enforce temporal adjacency, where semantically similar but non-adjacent (cross-block) queries are not shared.

a) *Selection Criteria:* Within each block, the first query serves as an initial reference and computes its critical indices across layers and heads. Following [25, 33] and the locality bias in **Observation 2**, selection budgets are allocated to three token groups: initial (sink) tokens, local tokens, and salient middle tokens. Let C_{sink} and C_{local} denote the numbers of sink and local tokens, respectively. At decoding step t , we obtain the middle set with a budget k by applying the top- k oracle over positions $[C_{\text{sink}}, t - C_{\text{local}}]$, excluding the sink and local regions. This yields $S_t^* = \{p_{t,i}\}_{i=1}^k$, where $p_{t,i}$ is sorted and selected in descending order of attention weight. The per-head critical index set is $\mathcal{C}_t = \{1, \dots, C_{\text{sink}}\} \cup S_t^* \cup \{t - C_{\text{local}} + 1, \dots, t\}$, with a total size $C = C_{\text{sink}} + k + C_{\text{local}}$.

b) *Similarity Criteria:* For a later query, if there exists an earlier query j whose cosine similarity exceeds a threshold τ , KV sharing is performed. We measure similarity as

$$\text{sim}(i, j) = \frac{\mathbf{q}_i^\top \mathbf{q}_j}{\|\mathbf{q}_i\| \|\mathbf{q}_j\|}. \quad (12)$$

If multiple candidates satisfy $\text{sim}(i, j) > \tau$, we choose the most recent such j to preserve adjacency. Varying τ trades throughput for accuracy.

c) *Neighboring Dilation:* Naive sharing ignores centroid drift (Eq. (11)) and yields fragmented critical sets (Figs. 2, 4), missing true positives for shared queries. We therefore dilate the m highest-weight indices in S_t^* (with $m \leq k$) by their $\pm r$ neighbors:

$$\hat{S}_t = S_t^* \cup \bigcup_{i=1}^m \{p_{t,i} + j \mid -r \leq j \leq r\}. \quad (13)$$

As shown in Fig. 4, dilation substantially increases true-positive overlap and achieves complete coverage compared to direct

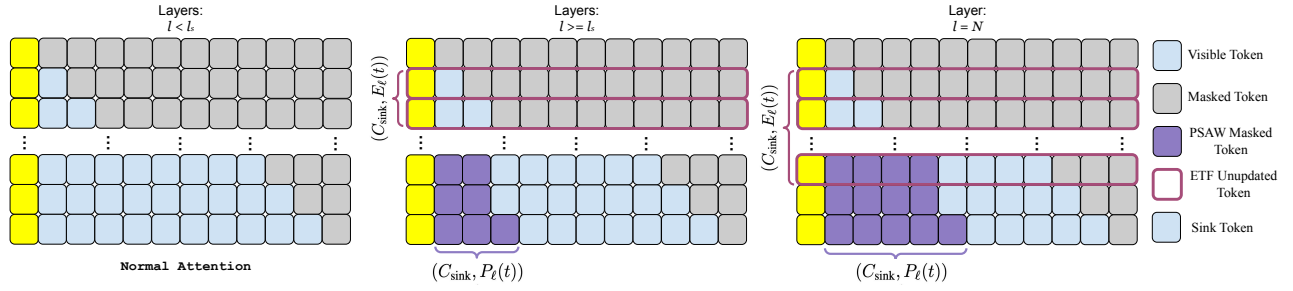


Fig. 5. **Visual illustration of PSAW and ETF in prefill stage.** When $\ell < \ell_s$, attention is unchanged. For $\ell \geq \ell_s$, both methods prune redundant computation: **PSAW** computes a per-step sliding window, so the set of **masked tokens** can vary across steps (columns); **ETF** applies a fixed prune range and freezes **earlier tokens** so they no longer update.

sharing. Moreover, restricting dilation to the top- m indices mitigates attention pollution from adding excessive low-weight tokens, as detailed in Sec. V-E1.

d) *Analysis:* Theoretically, CIS also turns Property 1 into a pre-hoc guarantee as proved in Theorem 2 (detailed in **Appendix A, A3**).

Theorem 2 (CIS Retained-Mass and MI Guarantee). *For a reference query q and its shared set \hat{S}_t dilated with $\pm r$ neighbors around the top- m winners ($m < k$), as in (13). Let $s(\tau)$ be any radius that covers the centroid drift implied by (11), for any later query \mathbf{q}' with $\text{sim}(\mathbf{q}, \mathbf{q}') \geq \tau$ (cosine similarity), if $r \geq s(\tau)$, then:*

$$\begin{aligned} \tau_{\text{pre}}(\mathbf{q}') &\geq \tau^*(\mathbf{q}') - \beta_{\text{th}}(\tau), \quad \beta_{\text{th}}(\tau) \leq 2 \Delta_{\text{att}}(\tau), \\ \text{where } \Delta_{\text{att}}(\tau) &:= \|A(\mathbf{q}') - A(\mathbf{q})\|_1 \leq \frac{2K_{\text{max}}}{\sqrt{d}} \sqrt{2-2\tau}. \end{aligned} \quad (14)$$

Consequently, the MI gap obeys the pre-hoc bound as in (9), where $\beta_{\text{th}}^{\text{CIS}}(\tau) = 2\Delta_{\text{att}}(\tau)$. If $r < s(\tau)$, the same holds with $2\Delta_{\text{att}}$ replaced by $2\Delta_{\text{att}}(\tau) + \varepsilon_{\text{drift}}(\mathbf{q}, \mathbf{q}'; m, r)$, where $\varepsilon_{\text{drift}}$ is the residual mass outside the chosen radius.

In short, by tying (τ, m, r) to Lipschitz continuity and the observed mean-shift of clustered indices, CIS achieves a controlled $\beta_{\text{th}}^{\text{CIS}}$ and therefore a tightened MI gap. Empirically, the mean-shift rate saturates once the prefix length exceeds a moderate scale; i.e., within a reasonably large block, cluster distributions of aligned queries become nearly identical. During experiments, $s \geq 8$ and $\text{sim} \geq 80\%$ can still satisfy competitive performance, which corresponds to aggressive sharing ratios.

B. Progressive Sliding Attention Window

PSAW progressively narrows each layer's attention window **during both prefill and decoding**. Consistent with **Observation 2**, attention is largely localized [25, 28]: apart from sink tokens, very early tokens receive negligible mass from later queries, and their content has already been propagated forward in lower layers. Thus, attending to them again in deeper layers is redundant.

Let $P_\ell(t)$ denote the earliest visible (non-sink) position at step t for layer ℓ , and let N be the total number of layer. We mask tokens in the index range $(C_{\text{sink}}, P_\ell(t))$, making the

visible set $\{1, \dots, C_{\text{sink}}\} \cup \{P_\ell(t), \dots, t\}$. Let ℓ_s be the layer depth at which pruning starts, we define

$$P_\ell(t) = \begin{cases} 0, & \ell < \ell_s \\ \lfloor (1 - \phi^\alpha \frac{\ell - \ell_s}{N - \ell_s}) t \rfloor, & \ell \geq \ell_s \end{cases} \quad (15)$$

where $\phi \in (0, 1)$ and $\alpha \geq 0$. For $\ell < \ell_s$, no pruning is applied to preserve early-information propagation. For $\ell \geq \ell_s$, the boundary $P_\ell(t)$ moves monotonically forward with depth because $\phi^\alpha \frac{\ell - \ell_s}{N - \ell_s}$ decreases as ℓ increases, yielding a progressively shrinking window. We adopt an exponentially decaying schedule rather than a linear one to better match attention locality biases, e.g., positional long-term decay [43] and softmax concentration, yielding tighter alignment with the empirical attention drop in long-range influence across layers (see **Appendix B**). The parameter α controls the decay schedule, while ϕ^α sets the top-layer truncation strength. A visualization of the PSAW mask is shown in Fig. 5, where **tokens in soft violet** indicate masked tokens.

Theoretically, by assuming attention probability mass with an exponential recency schedule beyond sink tokens, PSAW achieves a design-time certificate $\beta_{\text{th}}^{\text{PSAW}}$ and a tightened MI bound that improves as ϕ^α decreases or λ_ℓ grows.

C. Early Token Freezing

During **prefill**, ETF reduces computation by freezing an expanding prefix of early tokens in deeper layers. The intuition is that information from early tokens has already been propagated forward in shallower layers; further updating them yields diminishing returns. This implementation is also supported by the cross-layer redundancy (Sec. I) [34]. Let $E_\ell(t)$ denote the last frozen (non-sink) index at layer ℓ and step t . Tokens with positions in $(C_{\text{sink}}, E_\ell(t))$ are excluded from updates: they reuse their previous-layer hidden states, and their attention computations are skipped. Analogous to PSAW, we define

$$E_\ell(t) = \begin{cases} 0, & \ell < \ell_s \\ \lfloor (1 - \psi^\gamma \frac{\ell - \ell_s}{N - \ell_s}) t \rfloor, & \ell \geq \ell_s \end{cases} \quad (16)$$

where $\psi \in (0, 1)$ controls the final unfrozen fraction, and $\gamma > 0$ modulates the nonlinearity of the schedule. A visualization is provided in Fig. 5, where **tokens with reddish-purple edges** are frozen. Aligning PSAW, giving a small, depth-decaying budget $\beta_{\text{th}}^{\text{ETF}}$ and a correspondingly tight MI bound, ETF achieves

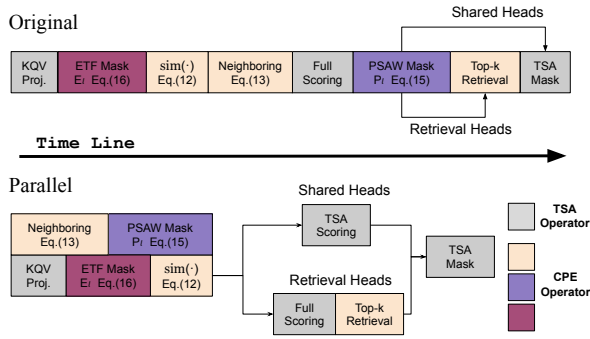


Fig. 6. **Parallel CPE acceleration.** *Top*: sequential baseline. *Bottom*: parallel design that fuses index manipulation with attention and directly computes TSA scoring for shared heads. **ETF** masking will be omitted in decoding.

a design-time guarantee by increasing ℓ_s or μ , as detailed in **Appendix D**.

D. Parallel Acceleration

a) Sequential execution: During inference, CPE executes TSA components in the order shown in Fig. 6 (Top). After KV projection (Eq. (1)), **ETF** freezes early tokens from further updates; during decoding, explicit ETF masking is unnecessary because only the newly generated position is updated. Next, **CIS** computes critical sets for shared heads using cosine gating and neighbor dilation (Eqs. (12) and (13)). We then perform full scoring and build the **PSAW** mask for redundant-attention pruning. For heads that still require retrieval, the top- k oracle is applied to obtain their critical sets. Finally, masks are applied so that each head attends only to its critical set.

b) Parallel acceleration: Many steps depend only on known quantities and can be prepared or executed in parallel (Fig. 6 (Bottom)). Specifically, previously computed critical sets are cached, and the **PSAW** mask is query-independent, allowing pre-computation. For **CIS**-shared heads, critical sets are already known, so full scoring is skipped and we compute attention only over valid indices (**TSA** scoring). Operations for shared heads and retrieval heads run concurrently, and the overall latency is determined by the slower branch.

V. EXPERIMENTS

A. Experimental Setup

We evaluate our CPE on two widely-used model families: LLaMA [22] and Mistral [35]. Specifically, we select LLaMA2-7B-Chat, LLaMA3-70B, and Mistral-7B for our experiments. As baselines, we select one TDO method H2O [25], two QAA algorithms: Quest [29] and DS [44], as well as a SOTA retrieval-based PoHS instantiation: HShare [33]. We report results on GSM8K [45], COQA [46], and LongBench [47].

In our CPE, we adopt the following default hyperparameters. For **CIS**, we set the similarity threshold $\tau = 0.8$, and apply dilation on the $m = \lfloor k/3 \rfloor$ highest-score indices with radius $r = 1$. Pruning and freezing of **PSAW** and **ETF** start from $\ell_s = \lfloor 3N/4 \rfloor$ for a model with N layers. **PSAW** uses $\phi = 0.7$ and $\alpha = 1$, while **ETF** uses $\psi = 0.5$ and $\gamma = 1$.

TABLE II
EVALUATION OF DIFFERENT METHODS ON GSM8K AND COQA. THE BEST RESULT (EXCLUDING ORIGIN) IN EACH COLUMN IS HIGHLIGHTED IN BOLD. COMP* REFERS TO THE THEORETICAL TIME COMPLEXITY FOR EACH METHOD TO SELECT CRITICAL KV CACHE TOKENS, WHERE $\mathcal{O}(1)$ DENOTES CONSTANT TIME COMPLEXITY, AND T REPRESENTS THE THEORETICAL COMPUTATION TIME FOR A DENSE ATTENTION MECHANISM.

Model	Method	$\hat{\rho}$	GSM8K \uparrow	COQA \uparrow	Comp* \downarrow	
LLaMA2 -7b-chat	Original	-	0.2297/0.2297	0.5997	-	
	H2O [25]	-	0.0986/0.0144	0.4952	$\mathcal{O}(1)$	
	Quest [29]	-	0.0478/0.0462	0.5713	0.1250T	
	DS [44]	-	0.1713/0.1706	0.5978	0.0625T	
	Hshare-1 [33]	0.281	0.1803/0.1703	0.5898	0.0180T	
	Hshare-2 [33]	0.125	0.1524/0.1145	0.5672	0.0080T	
	CIS (ours)		0.164	0.1842/0.1827	0.6085	0.0104T
			0.087	0.1804/0.1782	0.6072	0.0055T
			0.062	0.1759/0.1751	0.6068	0.0039T
	CIS* (ours)		0.161	0.1812/0.1804	0.6063	0.0103T
		0.084	0.1789/0.1782	0.6063	0.0047T	
		0.063	0.1736/0.1729	0.6083	0.0040T	
LLaMA3 -70b	Original	-	0.8067/0.8052	0.7085	-	
	DS [44]	-	0.7415/0.7392	0.7045	0.0625T	
	Hshare-1 [33]	0.281	0.7512/0.7437	0.7010	0.0180T	
	Hshare-2 [33]	0.125	0.7415/0.7346	0.6960	0.0080T	
	CIS (ours)		0.183	0.7613/0.7592	0.7045	0.0117T
			0.082	0.7553/0.7526	0.7021	0.0052T
			0.064	0.7528/0.7511	0.7003	0.0041T
	CIS* (ours)		0.179	0.7584/0.7556	0.7068	0.0114T
			0.079	0.7542/0.7527	0.7003	0.0050T
			0.061	0.7536/0.7504	0.7001	0.0038T
Mistral -7b	Original	-	0.3821/0.3813	0.6758	-	
	DS [44]	-	0.3262/0.3227	0.6693	0.0625T	
	Hshare-1 [33]	0.281	0.3199/0.3154	0.6560	0.0180T	
	Hshare-2 [33]	0.125	0.2818/0.2684	0.6387	0.0080T	
	CIS (ours)		0.194	0.3325/0.3302	0.6703	0.0124T
			0.088	0.3281/0.3275	0.6684	0.0056T
			0.065	0.3233/0.3201	0.6710	0.0041T
	CIS* (ours)		0.189	0.3292/0.3257	0.6691	0.0121T
			0.091	0.3216/0.3204	0.6714	0.0058T
			0.068	0.3204/0.3175	0.6754	0.0043T

Because **CIS** performs head-level KV sharing to avoid full retrieval, we define the *per-step retrieval ratio* $\rho_t = \frac{R_t}{H \cdot N}$ to measure the retrieval frequency, where R_t is the number of performed head-layer retrieval at step t , and $H \cdot N$ is the amount required by a naive top- k oracle. The ratio ρ_t is controlled by the **CIS** block size s and the similarity threshold τ . In reports, we present the averaged ratio $\hat{\rho} = \frac{1}{T} \sum^T \rho_t$ over the T generation steps.

B. Results on GSM8K and COQA

1) Datasets and Metrics: We perform zero-shot evaluation with LM-Eval on the GSM8K [45] and COQA [46] benchmarks. GSM8K comprises roughly 8 000 grade-school mathematics problems, whereas COQA targets multi-turn conversational question answering. The mean input lengths are about 500 tokens (GSM8K) and 2 000 tokens (COQA). Following prior work, we report both flexible and strict exact-match (EM) accuracy on GSM8K, and EM on COQA.

2) Inference Details: We apply **TSA** in the decoding stage and solely evaluate **CIS** as presented in Table II. We select a critical KV budget $C_t = 128$ [33]. For **CIS** and **Hshare**, we set $C_{\text{local}} = 32$, and $k = 88$ in the middle. Since **CIS** dilation incurs

TABLE III

EVALUATION OF DIFFERENT METHODS ON SIXTEEN ENGLISH DATASETS IN LONGBENCH AND THE BEST RESULT IN EACH ROW (EXCLUDING THE ORIGINAL) IS HIGHLIGHTED IN BOLD. HERE, THE RETRIEVAL COMPLEXITY OF H2O, QUEST, DS, AND HSHARE IS JUST THE SAME WITH TABLE II.

Dataset	Method											
	Original	H2O [25]	Quest [29]	DS [44]	HShare [33]		CIS (ours)		CIS* (ours)		CPE (ours)	
$\hat{\rho}$	-	-	-	-	0.281	0.125	0.177	0.083	0.164	0.085	0.174	0.079
MultiNews	26.22	24.88	26.49	26.30	26.05	25.22	26.47	25.98	26.18	26.40	26.11	26.02
Musique	8.65	6.24	4.62	8.72	8.42	8.09	8.47	6.98	8.74	8.68	8.69	7.50
HotpotQA	27.72	27.58	21.94	27.44	27.32	29.13	27.54	28.64	26.72	27.60	27.39	27.10
Qasper	21.88	17.32	16.96	20.98	20.12	19.60	21.24	21.18	20.87	20.79	20.94	21.63
2WikiMQA	31.18	31.38	29.42	32.01	31.46	31.43	32.51	30.78	30.05	30.70	29.06	31.15
Repo-P	52.14	51.81	50.24	48.44	50.79	51.63	50.99	50.03	50.65	50.88	51.64	51.12
TriviaQA	83.09	81.90	82.42	83.23	83.91	82.16	79.57	81.46	81.04	79.76	79.78	81.35
Trec	64.5	62.5	64.0	61.05	60.5	58.5	62.5	63.5	64.5	62.5	65.0	62.0
Qmsum	20.91	20.74	21.36	20.75	20.59	20.74	20.53	20.93	20.98	20.92	20.78	20.66
NarrativeQA	18.83	17.01	18.21	17.54	17.31	17.31	17.90	17.05	17.65	16.30	16.55	17.96
GovReport	26.55	23.45	25.46	27.04	25.85	25.85	26.63	26.39	26.07	26.39	25.63	25.78
LCC	58.26	56.55	56.74	54.87	56.23	56.11	55.35	54.43	54.89	55.10	55.62	54.22
PC	2.77	1.87	2.33	3.15	2.30	2.30	2.69	3.12	2.38	3.34	3.27	1.93
Samsun	41.01	40.18	40.91	41.30	39.77	40.02	40.96	40.52	39.04	39.68	40.11	40.19
PR-EN	6.5	5.0	6.5	6.0	6.0	6.0	8.5	7.0	6.0	9.5	6.0	6.0
MQA-EN	36.15	33.64	31.99	35.83	34.08	32.37	36.64	36.54	37.29	37.06	37.47	37.96
Average	32.90	31.38	31.35	32.11	31.97	31.49	32.40	32.15	32.06	32.22	32.11	32.02

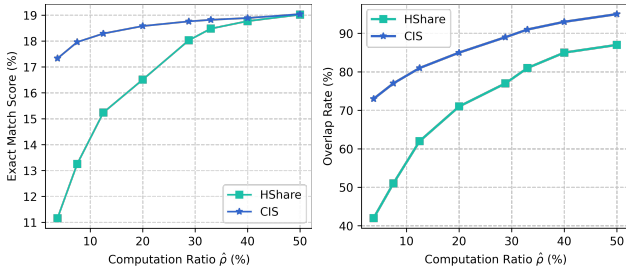


Fig. 7. CIS vs. HShare on GSM8K across computation ratios. Left: Exact-match score accuracy comparisons. Right: Overlap comparisons between each method’s retrieved critical set and the top- k oracle.

additional KV budget during sharing, we therefore additionally include a variant CIS*, which sets $k = 72$, yielding its average budget close to 128. We choose $s \in \{8, 16, 20\}$ to vary $\hat{\rho}$.

3) *Result Analysis*: As shown in Table II, CIS and its budget-matched variant CIS* consistently deliver a superior accuracy–efficiency trade-off to PoHS baselines on GSM8K and COQA. On LLaMA-2-7B-Chat, CIS at low selection cost already surpasses SOTA HShare, i.e., 40–55% lower complexity at higher accuracy. The advantage widens on LLaMA-3-70B with deeper layers, consistent with reduced cross-layer error accumulation under sharing. CIS* still outperforms HShare at matched budgets, isolating selection *quality* rather than capacity as the driver of the gains. Efficiency is materially better. For instance, on LLaMA-3-70B, CIS uses 0.0052 T selection cost versus DS’s 0.0625 T .

To further evaluate the accuracy-efficiency trade-offs of CIS, we compare the results of HShare and CIS under different computation ratios on GSM8K. As shown in Fig. 7(left), when computation ratio is below 30%, the performance of HShare degrades sharply, while CIS maintains high accuracy. From the perspective of retrained attention mass, Fig. 7(right) shows that the average overlap of HShare collapses at low computation

ratio. These results further demonstrate that the selection quality of CIS is much better than HShare under aggressive sharing.

C. Longbench

1) *Datasets and Metrics*: LongBench contains sixteen English tasks spanning code completion, few-shot learning, document-level QA, summarisation, and synthetic reasoning. We adhere to the official evaluation protocol: MultiNews, Qmsun, GovReport, Samsun with rouge score; Musique, HotpotQA, Qasper, 2WikiMQA, TriviaQA, NarrativeQA, MultifieldQA-EN (MQA) with F1 score; trec with classification accuracy; Passage-Count (PC), Passage-Retrieval-EN (PR-EN) exact-match accuracy; RepoBench-P (Repo-P) and LCC with similarity score.

2) *Inference Details*: All baselines apply TSA only during decoding and retain a 512 KV budget, with a sparsity ratio of $\approx 1/8$. For HShare and CIS we set $C_{\text{sink}}=16$, $C_{\text{local}}=64$, and $k=432$. With CIS’s neighbor dilation, the effective shared-head set averages 547.5 tokens. To enable a budget-matched comparison, CIS* reduces the middle-budget to $k=388$, equalizing the average KV budget processed during decoding to 512. For the combined system CPE, we use $k=432$ and also activate PSAW and ETF during *prefill*. Reductions achieved in prefill are not counted toward the decoding-budget metric, so CPE further lowers prefill cost in addition to the standard decoding-only comparison. We use block size $s \in \{8, 16\}$.

3) *Results Analysis*: Across sparse baselines, CIS attains the best average while using substantially lower retrieval than SOTA HShare, as shown in Table III. Specifically, CIS achieves the highest non-dense average, 32.40, at a moderate retrieval ratio $\hat{\rho}=0.177$, surpassing HShare’s best 31.97 at $\hat{\rho}=0.281$ with 37% less retrieval. Moreover, CIS* remains competitive with HShare while substantially reducing retrieval, indicating that gains stem from selection quality rather than capacity. CPE preserves this competitiveness (32.11) while additionally reducing prefill cost.

TABLE IV

ATTENTION OPERATOR LATENCY (MS \downarrow) OF DIFFERENT METHODS ACROSS VARIOUS BATCH SIZES AND SEQUENCE LENGTHS. LOWER VALUES INDICATE BETTER PERFORMANCE. HSHARE-0 CORRESPONDS TO HSHARE(3/4-3/4-1/2), AND HSHARE-1 TO HSHARE(1/2-1/2-1/2). THE NUMBER FOLLOWING EACH OF OUR METHODS INDICATES THE BLOCK SIZE s USED IN CIS.

BS	SeqLen	Flash	H2O [25]	Quest [29]	DS [44]	HShare-0 [33]	HShare-1 [33]	CIS-8	CIS-16	CPE-8	CPE-16
8	1k	0.230	0.088	0.200	0.141	0.124	0.090	0.116	0.083	0.092	0.078
	2k	0.830	0.093	0.460	0.241	0.160	0.120	0.147	0.106	0.144	0.095
	4k	1.630	0.470	0.850	0.733	0.570	0.530	0.534	0.501	0.506	0.469
16	1k	0.440	0.089	0.280	0.233	0.120	0.093	0.113	0.081	0.089	0.075
	2k	1.630	0.110	0.770	0.422	0.230	0.190	0.214	0.178	0.196	0.165
	4k	3.230	0.850	2.21	1.350	1.041	0.990	0.953	0.869	0.904	0.821

TABLE V

THROUGHPUT (\uparrow) OF DIFFERENT METHODS ACROSS VARIOUS BATCH SIZES AND SEQUENCE LENGTHS. HSHARE-0 CORRESPONDS TO HSHARE(3/4-3/4-1/2), AND HSHARE-1 TO HSHARE(1/2-1/2-1/2). THE NUMBER FOLLOWING EACH OF OUR METHODS INDICATES THE BLOCK SIZE s USED IN CIS.

BS	SeqLen	GPT-Fast	H2O [25]	Quest [29]	DS [44]	HShare-0 [33]	HShare-1 [33]	CIS-8	CIS-16	CPE-8	CPE-16
8	1k	228	240	228	228	231	235	233	236	238	244
	2k	188	234	206	213	222	226	216	224	225	233
	4k	118	228	152	201	214	217	216	220	219	227
16	1k	374	441	410	423	430	439	433	443	441	449
	2k	233	416	287	360	398	411	402	415	412	421
	4k	136	396	175	286	350	365	352	364	362	384

Although prefill reductions are not counted in the decoding budget, CPE still ties or wins on several tasks, showing that pruning and freezing early tokens remove redundant compute without harming downstream reasoning—consistent with the error control guaranteed by PrHS.

D. Efficiency Evaluation

1) *Inference Detail*: Following prior work [44, 33], we measure (i) self-attention operator latency and (ii) end-to-end throughput in the decoding stage. Experiments use LLaMA-2-7B-Chat on a server with an Intel Xeon Platinum 8336C CPU, a single NVIDIA A100 GPU, and 120 GB RAM. For the operator benchmark, FlashAttention-2 (Flash) [48] serves as the dense baseline. For the end-to-end benchmark, we use GPT-fast [49] as the dense baseline and replace its attention module with our TSA implementation. We test batch sizes 8, 16 and sequence lengths 1k–4k at a token sparsity ratio of 1/8. We report results for CIS and CPE (CIS+PSAW; ETF is prefill-only) with block sizes $s \in \{8, 16\}$. Because CIS confines sharing within a block, the extra cache is minimal, and the added per-step bookkeeping is bounded by $\mathcal{O}(Hsk)$.

2) Results Analysis:

a) *Operator latency*: As shown in Table IV, CPE-16 delivers the fastest kernel at both small and long contexts for each batch size (BS). At 2k tokens and BS=16, it attains a $9.9\times$ speedup over Flash. At 4k tokens, relative to the SOTA PoHS baseline, HShare-1, CPE-16 reduces latency by 11.5% (BS=8) and 17.1% (BS=16), and it outperforms DS by up to 39% at BS=16. H2O is competitive at 2k, where its ultra-light TDO pattern minimizes overhead. CIS alone also confers a clear advantage: at BS=16, CIS-16 is 11–15% faster than HShare-1. The pattern is consistent with head-level sharing plus PSAW amortizing their $\mathcal{O}(Hsk)$ bookkeeping once the

GPU is well utilized, leaving reduced active KV compute as the runtime driver.

b) *End-to-end throughput*: Operator gains translate to real decoding speed, as shown in Table V. Relative to GPT-Fast, CPE-16 reaches $2.82\times$ at BS=16, 4k. At BS=16 and 1–2k, CPE-16 achieves the highest throughput, edging out H2O; at BS=8, it leads at 1k and effectively ties H2O at longer contexts. As batch size and sequence length grow, the gap between operator-level and end-to-end gains narrows due to non-attention bottlenecks (MLPs, sampling), yet CPE consistently ranks first or near-first across realistic loads, with $s=16$ providing the strongest throughput.

c) *Effect of block size*: Across settings, $s=16$ is consistently faster than $s=8$ for both CIS and CPE. Larger boundaries reduce launch and index-management overhead and allow sharing decisions to persist longer, so the small increase in per-block work is negligible compared to better kernel efficiency. This argues for $s=16$ as the default in high-throughput deployments.

E. Further Analysis

1) *CIS Dilation*: We assess CIS dilation using the CIS* configurations from Sec. V-C, varying the number of top indices dilated m . As shown in Fig. 8, the number of *additional* tokens beyond the top- k set remains small for moderate m ; dilation overhead grows gradually as m increases, and the added tokens are predominantly low-importance. Inspecting shared queries explains this behavior as follows. Their most influential critical tokens are tightly clustered and spatially stable, so dilation contributes few extra indices. In contrast, when the budget begins to include low-score tokens, these indices are irregular and scattered, and dilation substantially inflates the set. This motivates restricting dilation to a top fraction of retrieved

TABLE VI

HYPERPARAMETER TUNING ON LLAMA2-CHAT-7B FOR CPE. THE COQA SETTING FOR CIS FOLLOWS THE CIS* CONFIGURATION, AND HYPERKV FOLLOWS THE HYPERKV CONFIGURATION, AS DESCRIBED IN SEC. V-B. WIKITEXT PERPLEXITY (PPL) IS MEASURED ONLY DURING THE PREFILLING STAGE. THE AVG.TOKEN MEASURES THE AVERAGE PROCESSED TOKENS PER HEAD ONLY IN THE DECODING STAGE.

Methods	s	τ	r	ϕ	ψ	α	γ	$\hat{\rho}$	Avg. Token	Wiki PPL	GSM8K(flexible)	COQA(EM/F1)
CIS	4	0.8	1	-	-	-	-	0.301	124	-	0.1834	0.6023 / 0.7632
	8	0.7	1	-	-	-	-	0.152	131	-	0.1801	0.6090 / 0.7648
	8	0.8	2	-	-	-	-	0.184	167	-	0.1653	0.6083 / 0.7650
	32	0.8	1	-	-	-	-	0.0046	136	-	0.1693	0.6080 / 0.7641
PSAW	-	-	-	0.5	-	1	-	-	-	6.120	0.1896	0.5925 / 0.7568
	-	-	-	0.7	-	1.5	-	-	-	6.113	0.1803	0.5938 / 0.7573
ETF	-	-	-	-	0.5	-	1.5	-	-	6.162	0.1864	0.5962 / 0.7563
	-	-	-	-	0.4	-	1	-	-	6.156	0.1883	0.5962 / 0.7537
CPE	8	0.8	2	0.7	0.5	1.2	1.2	0.176	166	6.148	0.1348	0.5998 / 0.7591
	32	0.8	1	0.7	0.5	1	1	0.0044	133	6.136	0.1634	0.5965 / 0.7572

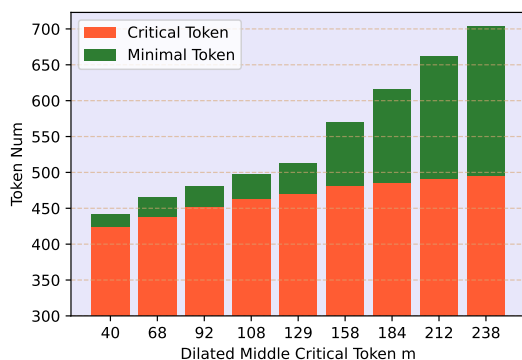


Fig. 8. Effect of CIS dilation on LongBench NarrativeQA. The stacked bar shows the average processed KV set: the orange segment counts tokens that also appear in the top- k oracle (budget 512, following Sec. V-C), while the green segment counts minimal tokens not in the top- k set.

tokens. In practice, the expanded set also overlaps heavily with the remaining retrieved indices, further limiting redundancy.

2) Hyperparameter Tuning:

a) Setting: We tune the key knobs of our compression pipeline in Table VI. For CIS, we adopt the CIS* configuration from Sec. V-B and vary the block size s , similarity threshold τ , and neighbor radius r . For PSAW and ETF in isolation, we apply them on dense attention, fix $\ell_s = \lfloor 3N/4 \rfloor$, and control pruning/freezing aggressiveness via (ϕ, α) for PSAW and (ψ, γ) for ETF; PSAW is active in both prefill and decoding. For CPE, we combine all three components, adding PSAW and ETF to CIS under TSA. We report: the averaged computation ratio $\hat{\rho}$, the average processed tokens per head in decoding (Avg.Token), prefill-only WikiText perplexity (PPL), and task accuracy on GSM8K (flex) and COQA (EM/F1).

b) CIS: Varying (s, τ, r) reveals the accuracy–efficiency trade-off. Smaller s increases retrieval frequency (higher $\hat{\rho}$), whereas enlarging to $s=32$ drives the retrieval ratio down to $\hat{\rho}=0.0046$ with only a modest GSM8K accuracy drop; COQA remains notably stable across all s . At fixed $s=8$, increasing the dilation radius to $r=2$ substantially enlarges the active set but yields negligible accuracy change on both GSM8K and COQA; inspection shows that the added neighbors often include low-importance tokens, perturbing the attention-mass distribution without benefits. Slightly loosening τ has

TABLE VII

VARIANTS OF CIS ON THE SIMILARITY DESIGNS. THE MODEL IS LLAMA2-7B-CHAT.

Method	s	GSM8K (flexible/strict)	COQA
Key	8	0.1547 / 0.1482	0.5613
	16	0.1405 / 0.1334	0.5608
Hidden	8	0.1303 / 0.1289	0.5416
	16	0.1121 / 0.1108	0.5214

little effect on accuracy. Overall, s is the dominant lever for efficiency, while τ and r offer fine-grained control of recall versus budget.

c) PSAW: Prefill pruning is gentle on language modeling quality and downstream accuracy. Increasing aggressiveness from $(\phi=0.5, \alpha=1)$ to $(\phi=0.7, \alpha=1.5)$ barely changes WikiText PPL, and COQA is essentially unchanged, while GSM8K (flexible match) decreases only slightly.

d) ETF: Freezing during prefill shows similarly small effects. Adjusting from $(\psi=0.5, \gamma=1.5)$ to $(\psi=0.4, \gamma=1)$ yields virtually identical PPL and a tiny trade between GSM8K and COQA. ETF is therefore a stable knob for further prefill savings and slightly milder freezing is a safe default setting.

e) CPE: Combining CIS with PSAW and ETF preserves efficiency while keeping quality competitive. With aggressive dilation ($r=2$), GSM8K dips to 0.1348. Increasing block size and reducing dilation to $r=1$ lowers selection frequency and trims Avg. Token by $\sim 20\%$, recovering GSM8K to 0.1634 with COQA nearly unchanged. Overall, CPE performs best with moderate–large blocks, restricted dilation ($r=1$), and mild PSAW/ETF schedules.

3) Similarity Ablations: We explore alternative similarity metrics for CIS derived from different representations. Concretely, we replace the default cosine similarity between query embeddings (Eq. 12) with cosine similarity computed on (i) hidden states \mathbf{x} and (ii) key embeddings \mathbf{k} , and evaluate under the CIS* configuration in Sec. V-B. As shown in Table VII, both variants reduce accuracy, with the hidden-state metric degrading most. This indicates that the query, key, and hidden-state spaces emphasize distinct semantics; temporal semantic proximity for CIS is best captured in the query space, whereas

measuring similarity in \mathbf{x} or \mathbf{k} misaligns clusters and harms selection quality.

VI. CONCLUSION

In this paper, we propose Pre-hoc Sparsity (PrHS) framework, and derive an upper bound on the mutual-information (MI) loss based on the dropped attention mass. By tightening the MI bound towards the top- k oracle, selectors under PrHS can achieve near-oracle KV compression. We propose **CPE** that instantiate three orthogonal modules under PrHS: *Clustered Indices Sharing* (CIS), *Progressive Sliding Attention Window* (PSAW), and *Early Token Freezing* (ETF). CIS expands the highest-score indices in each shared critical set to its neighbors, achieving high recall and preserving accuracy even at aggressive ($\geq 90\%$) sharing ratios. PSAW and ETF further amplify sparsity by **masking tokens** that lie outside a dynamically sliding context window and **freezing tokens** whose updates have converged, thereby eliminating redundant computation with negligible performance loss. Extensive evaluations on GSM8K, COQA, and LongBench demonstrate that CPE (i) matches dense baselines in accuracy under high attention sparsity, (ii) reduces retrieval complexity by up to $3\times$ than recent SOTA HShare [33] with even better performance, (iii) delivers up to a $9.9\times$ latency speed-up over FlashAttention and a $2.8\times$ throughput gain over GPT-Fast. These results confirm CPE as an effective and broadly applicable solution for efficient long-context inference in LLMs.

VII. UNIFIED INFORMATION BOUNDS

A. Setup

We consider the minimal unit of the information bound and fix both the layer and the head. Following the softmax attention distribution defined in Sec. II-A and Eq. 2, for a query \mathbf{q} , with $\mathbf{K} = [\mathbf{k}_1, \dots, \mathbf{k}_L]$ and $\mathbf{V} = [\mathbf{v}_1, \dots, \mathbf{v}_L]$ denote keys/values for a context of length L , we introduce the *latent index* random variable

$$T \in [L], \quad \mathbb{P}(T = i | \mathbf{q}, \mathbf{K}) = A_i(\mathbf{q}), \quad (17)$$

and the routed value \mathbf{V}_T for token-sparse attention. Let $I_{\text{full}}(\mathbf{q})$ denote the (per-query) information carried by full attention, for a size- n selector $\mathcal{S} \subseteq [L]$, the retained attention mass $\tau_{\mathcal{S}}(\mathbf{q})$ and dropped attention mass $\delta_{\mathcal{S}}$ are defined as:

$$\tau_{\mathcal{S}}(\mathbf{q}) = \sum_{i \in \mathcal{S}} A_i(\mathbf{q}), \quad \delta_{\mathcal{S}}(\mathbf{q}) = 1 - \tau_{\mathcal{S}}(\mathbf{q}). \quad (18)$$

Let $\tilde{A}_{\mathcal{S}}(\mathbf{q})$ be the truncated/renormalized distribution (follow the normalization of the softmax)

$$\tilde{A}_i(\mathbf{q}) = \begin{cases} A_i(\mathbf{q})/\tau_{\mathcal{S}}(\mathbf{q}), & i \in \mathcal{S}, \\ 0, & \text{otherwise,} \end{cases} \quad T_{\mathcal{S}} \sim \tilde{A}_{\mathcal{S}}(\mathbf{q}). \quad (19)$$

Denote by $I_{\mathcal{S}}(\mathbf{q})$ the information of the token-sparse channel that keeps indices in \mathcal{S} and routes $\mathbf{V}_{T_{\mathcal{S}}}$. And let $\mathcal{S}^*(\mathbf{q}) = \text{Top}_n(A(\mathbf{q}))$ be the top- n oracle set with

$$\tau^*(\mathbf{q}) = \tau_{\mathcal{S}^*}(\mathbf{q}), \quad \delta^*(\mathbf{q}) = 1 - \tau^*(\mathbf{q}). \quad (20)$$

Remark 1 (We bound information via the index channel). *By data processing along $(\mathbf{K}, \mathbf{V}) \rightarrow T \rightarrow \mathbf{V}_T$, it suffices (and is*

conservative) to control the loss in mutual information induced by truncating T ; this yields bounds for $I_{\text{full}}(\mathbf{q}) - I_{\mathcal{S}}(\mathbf{q})$.

B. Two universal technical lemmas

Lemma 1 (Total-variation of truncation). *For any size- n selector \mathcal{S} ,*

$$\|A(\cdot | \mathbf{q}) - \tilde{A}_{\mathcal{S}}(\cdot | \mathbf{q})\|_{\text{TV}} = \delta_{\mathcal{S}}(\mathbf{q}). \quad (21)$$

Proof. Write $P = A(\cdot | \mathbf{q})$ and $Q = \tilde{A}_{\mathcal{S}}(\cdot | \mathbf{q})$. Then

$$\begin{aligned} \|P - Q\|_{\text{TV}} &= \frac{1}{2} \sum_{i=1}^L |P_i - Q_i| \\ &= \frac{1}{2} \left(\sum_{i \notin \mathcal{S}} P_i + \sum_{i \in \mathcal{S}} |P_i - P_i/\tau_{\mathcal{S}}| \right) \\ &= \frac{1}{2} (\delta_{\mathcal{S}} + \delta_{\mathcal{S}}) = \delta_{\mathcal{S}}. \end{aligned}$$

□

Lemma 2 (Continuity of mutual information (MI) under TV perturbations). *Let $\mathbf{X} = (\mathbf{K}, \mathbf{V})$ and consider two channels from \mathbf{X} to an output random variable $\mathbf{Y} \equiv \mathbf{V}_T$ and $\mathbf{Y}' \equiv \mathbf{V}_{T_{\mathcal{S}}}$, where for each $\mathbf{x} = (\mathbf{k}, \mathbf{v})$, the conditional law $T|\mathbf{X} = \mathbf{x}$ is $A(\cdot | \mathbf{q}, \mathbf{k})$ and $T_{\mathcal{S}}|\mathbf{X} = \mathbf{x}$ is the truncated/renormalized $\tilde{A}_{\mathcal{S}}(\cdot | \mathbf{q}, \mathbf{k})$. Assume the (uniform) total-variation gap*

$$\begin{aligned} \sup_{\mathbf{x}} \|\mathbb{P}(T \in \cdot | \mathbf{X} = \mathbf{x}) - \mathbb{P}(T_{\mathcal{S}} \in \cdot | \mathbf{X} = \mathbf{x})\|_{\text{TV}} \\ = \delta_{\mathcal{S}}(\mathbf{q}) =: \delta \in [0, 1]. \end{aligned} \quad (22)$$

Then, for every input law $\mathbf{P}_{\mathbf{X}}$,

$$|I(\mathbf{X}; \mathbf{Y}) - I(\mathbf{X}; \mathbf{Y}')| \leq 2 \left[h_b(\delta) + \delta \log L \right],$$

where I is the MI measure, h_b is the binary entropy function. Consequently,

$$0 \leq I_{\text{full}}(\mathbf{q}) - I_{\mathcal{S}}(\mathbf{q}) \leq 2 \left[h_b(\delta_{\mathcal{S}}(\mathbf{q})) + \delta_{\mathcal{S}}(\mathbf{q}) \log L \right].$$

Proof. Step 1: Per- \mathbf{x} support size and induced kernels. Fix $\mathbf{x} = (\mathbf{k}, \mathbf{v})$. The map $t \mapsto \mathbf{v}_t$ is deterministic (given \mathbf{x}), hence $\mathbf{Y}|\mathbf{X} = \mathbf{x}$ and $\mathbf{Y}'|\mathbf{X} = \mathbf{x}$ are obtained by pushing forward the probability mass function (pmfs) $A(\cdot | \mathbf{q}, \mathbf{k})$ and $\tilde{A}_{\mathcal{S}}(\cdot | \mathbf{q}, \mathbf{k})$ through a map with image of size at most L :

$$\mathbf{Y}_{\mathbf{x}} = \{\mathbf{v}_1, \dots, \mathbf{v}_L\}, \quad |\mathbf{Y}_{\mathbf{x}}| \leq L.$$

Let $W_{\mathbf{x}}$ and $\tilde{W}_{\mathbf{x}}$ denote the conditional pmfs of $\mathbf{Y}|\mathbf{X} = \mathbf{x}$ and $\mathbf{Y}'|\mathbf{X} = \mathbf{x}$, respectively. Total variation cannot increase under measurable mappings, so

$$\|\mathbf{W}_{\mathbf{x}} - \tilde{\mathbf{W}}_{\mathbf{x}}\|_{\text{TV}} \leq \|A(\cdot | \mathbf{q}, \mathbf{k}) - \tilde{A}_{\mathcal{S}}(\cdot | \mathbf{q}, \mathbf{k})\|_{\text{TV}} \leq \delta. \quad (23)$$

Step 2: Continuity of (conditional) entropy at fixed \mathbf{x} . For pmfs P, Q on a finite alphabet of size m with $\|P - Q\|_{\text{TV}} \leq \varepsilon$, the classical continuity bound for the Shannon entropy gives

$$\begin{aligned} |H(P) - H(Q)| &\leq h_b(\varepsilon) + \varepsilon \log(m - 1) \\ &\leq h_b(\varepsilon) + \varepsilon \log m. \end{aligned} \quad (24)$$

Applying (24) to $(P, Q) = (\mathbf{W}_{\mathbf{x}}, \tilde{\mathbf{W}}_{\mathbf{x}})$ with $m = |\mathbf{Y}_{\mathbf{x}}| \leq L$ and $\varepsilon \leq \delta$ from (23), we obtain

$$|H(\mathbf{Y}|\mathbf{X} = \mathbf{x}) - H(\mathbf{Y}'|\mathbf{X} = \mathbf{x})| \leq h_b(\delta) + \delta \log L. \quad (25)$$

Averaging over \mathbf{X} yields

$$|H(\mathbf{Y}|\mathbf{X}) - H(\mathbf{Y}'|\mathbf{X})| \leq h_b(\delta) + \delta \log L. \quad (26)$$

Step 3: Continuity of the marginal entropy. Let $P_{\mathbf{Y}}$ and $P_{\mathbf{Y}'}$ be the marginals induced by $P_{\mathbf{X}}$ and the kernels $\{\mathbf{W}_{\mathbf{x}}\}, \{\widetilde{\mathbf{W}}_{\mathbf{x}}\}$: $P_{\mathbf{Y}}(\cdot) = \sum_{\mathbf{x}} P_{\mathbf{X}}(\mathbf{x}) \mathbf{W}_{\mathbf{x}}(\cdot)$ and $P_{\mathbf{Y}' }(\cdot) = \sum_{\mathbf{x}} P_{\mathbf{X}}(\mathbf{x}) \widetilde{\mathbf{W}}_{\mathbf{x}}(\cdot)$. Then

$$\begin{aligned} \|P_{\mathbf{Y}} - P_{\mathbf{Y}'}\|_{\text{TV}} &= \frac{1}{2} \sum_{\mathbf{y}} \left| \sum_{\mathbf{x}} P_{\mathbf{X}}(\mathbf{x}) (\mathbf{W}_{\mathbf{x}}(\mathbf{y}) - \widetilde{\mathbf{W}}_{\mathbf{x}}(\mathbf{y})) \right| \\ &\leq \frac{1}{2} \sum_{\mathbf{x}} P_{\mathbf{X}}(\mathbf{x}) \sum_{\mathbf{y}} |\mathbf{W}_{\mathbf{x}}(\mathbf{y}) - \widetilde{\mathbf{W}}_{\mathbf{x}}(\mathbf{y})| \\ &= \sum_{\mathbf{x}} P_{\mathbf{X}}(\mathbf{x}) \|\mathbf{W}_{\mathbf{x}} - \widetilde{\mathbf{W}}_{\mathbf{x}}\|_{\text{TV}} \leq \delta, \end{aligned}$$

where the last step uses (23). Since the (per- \mathbf{x}) images have size $\leq L$, the union of supports $\text{supp}(P_{\mathbf{Y}}) \cup \text{supp}(P_{\mathbf{Y}'})$ also has effective cardinality at most L for the purpose of the continuity bound.² Therefore, applying (24) to $(P_{\mathbf{Y}}, P_{\mathbf{Y}'})$ yields

$$|H(\mathbf{Y}) - H(\mathbf{Y}')| \leq h_b(\delta) + \delta \log L. \quad (27)$$

Step 4: Mutual information difference. Using the chain rule $I(\mathbf{X}; \mathbf{Y}) = H(\mathbf{Y}) - H(\mathbf{Y}|\mathbf{X})$ and combining (26)–(27),

$$\begin{aligned} &|I(\mathbf{X}; \mathbf{Y}) - I(\mathbf{X}; \mathbf{Y}')| \\ &\leq |H(\mathbf{Y}) - H(\mathbf{Y}')| + |H(\mathbf{Y}'|\mathbf{X}) - H(\mathbf{Y}|\mathbf{X})| \\ &\leq 2[h_b(\delta) + \delta \log L]. \end{aligned} \quad (28)$$

which is the desired inequality.

Step 5: Consequence for $I_{\text{full}}(\mathbf{q}) - I_{\mathcal{S}}(\mathbf{q})$. By construction, the "full attention" and "token-sparse attention" channels differ only in the selector distribution (full T vs. truncated $T_{\mathcal{S}}$), while the downstream map $(\mathbf{X}, T) \mapsto \mathbf{Y}$ is the same. Thus the loss in the information measure realized through \mathbf{Y} is bounded by the above calculation with $\delta = \delta_{\mathcal{S}}(\mathbf{q})$, giving

$$0 \leq I_{\text{full}}(\mathbf{q}) - I_{\mathcal{S}}(\mathbf{q}) \leq 2[h_b(\delta_{\mathcal{S}}(\mathbf{q})) + \delta_{\mathcal{S}}(\mathbf{q}) \log L]. \quad \square$$

At this point, we have completed the full derivation of the information bound for token-sparse attention and incorporated a unified measure $\delta_{\mathcal{S}}$, related to dropped attention mass, to quantify the magnitude of information loss.

VIII. INFORMATION BOUNDS OF TOKEN-SPARSE ATTENTION

For the selector of the token-sparse attention, we have:

Proposition 1 (Universal MI bounds & KL variant). *For any selector \mathcal{S} ,*

$$0 \leq I_{\text{full}}(\mathbf{q}) - I_{\mathcal{S}}(\mathbf{q}) \leq 2[h_b(\delta_{\mathcal{S}}(\mathbf{q})) + \delta_{\mathcal{S}}(\mathbf{q}) \log L]. \quad (\text{U1})$$

Moreover,

$$I_{\mathcal{S}}(\mathbf{q}) \geq I_{\text{full}}(\mathbf{q}) - \log \frac{1}{\tau_{\mathcal{S}}(\mathbf{q})}. \quad (\text{U2})$$

²It suffices that each mixture component lives on an alphabet of size $\leq L$; the bound (24) only needs a uniform cardinality upper bound.

Proof. The first inequality is Lemma 2. For (U2),

$$D_{\text{KL}}(\widetilde{A}_{\mathcal{S}} \| A) = \sum_{i \in \mathcal{S}} \frac{A_i}{\tau_{\mathcal{S}}} \log \frac{A_i/\tau_{\mathcal{S}}}{A_i} = \log \frac{1}{\tau_{\mathcal{S}}}.$$

A variational (Donsker–Varadhan) representation of MI plus data processing upper bounds the MI drop by this KL. \square

A. Oracle top- k selection

Theorem 3 (Oracle top- k information bound). *Let $\mathcal{S}^*(\mathbf{q}) = \text{Top}_n(A(\mathbf{q}))$ and $\delta^*(\mathbf{q}) = 1 - \tau^*(\mathbf{q})$. Then*

$$0 \leq I_{\text{full}}(\mathbf{q}) - I_{\mathcal{S}^*}(\mathbf{q}) \leq 2[h_b(\delta^*(\mathbf{q})) + \delta^*(\mathbf{q}) \log L], \quad (\text{O1})$$

and

$$I_{\mathcal{S}^*}(\mathbf{q}) \geq I_{\text{full}}(\mathbf{q}) - \log \frac{1}{\tau^*(\mathbf{q})}. \quad (\text{O2})$$

Proof. Among all $|S|=n$, \mathcal{S}^* maximizes $\tau_{\mathcal{S}}$ and minimizes $\delta_{\mathcal{S}}$ by additivity of $\sum_{i \in \mathcal{S}} A_i$. Apply Proposition 1 with $\mathcal{S}=\mathcal{S}^*$. \square

B. Post-hoc sparsity

Post-hoc methods construct a *surrogate* probability vector $\widehat{A}_D(\mathbf{q})$ from posterior side information D and select

$$\mathcal{S}_D(\mathbf{q}) = \text{Top}_n(\widehat{A}_D(\mathbf{q})).$$

Define the *posterior-bias (mass gap)* β_D

$$\beta_D(\mathbf{q}) \stackrel{\text{def}}{=} \tau^*(\mathbf{q}) - \tau_{\mathcal{S}_D}(\mathbf{q}) = \delta_{\mathcal{S}_D}(\mathbf{q}) - \delta^*(\mathbf{q}) \geq 0. \quad (\text{PB})$$

Measure the surrogate misfit by

$$\varepsilon_D(\mathbf{q}) \stackrel{\text{def}}{=} \frac{1}{2} \|A(\mathbf{q}) - \widehat{A}_D(\mathbf{q})\|_1 = \|A(\mathbf{q}) - \widehat{A}_D(\mathbf{q})\|_{\text{TV}}. \quad (29)$$

Lemma 3 (Mis-scoring \Rightarrow mass loss). *Let $\mathcal{S}^* = \text{Top}_n(A)$ and $\mathcal{S}_D = \text{Top}_n(\widehat{A}_D)$. Then*

$$\beta_D(\mathbf{q}) \leq 2\varepsilon_D(\mathbf{q}) \iff \delta_{\mathcal{S}_D}(\mathbf{q}) \leq \delta^*(\mathbf{q}) + 2\varepsilon_D(\mathbf{q}). \quad (\text{MassLoss})$$

Proof. For any $S \subseteq [L]$, $|A(S) - \widehat{A}_D(S)| \leq \varepsilon_D$. Since $\widehat{A}_D(\mathcal{S}_D) \geq \widehat{A}_D(\mathcal{S}^*)$,

$$A(\mathcal{S}_D) \geq \widehat{A}_D(\mathcal{S}_D) - \varepsilon_D \geq \widehat{A}_D(\mathcal{S}^*) - \varepsilon_D \geq A(\mathcal{S}^*) - 2\varepsilon_D.$$

Thus $\tau_{\mathcal{S}_D} \geq \tau^* - 2\varepsilon_D$ and the claim follows. \square

Theorem 4 (Unified post-hoc information bound). *For any post-hoc selector \mathcal{S}_D , let $\delta_{\varepsilon_D}(\mathbf{q}) = \delta^*(\mathbf{q}) + 2\varepsilon_D(\mathbf{q})$,*

$$I_{\text{full}}(\mathbf{q}) - I_{\text{post}}(\mathbf{q}) \leq 2[h_b(\delta_{\varepsilon_D}(\mathbf{q})) + \delta_{\varepsilon_D}(\mathbf{q}) \log L], \quad (\text{P1})$$

and

$$I_{\text{post}}(\mathbf{q}) \geq I_{\text{full}}(\mathbf{q}) - \log \frac{1}{1 - \delta_{\varepsilon_D}(\mathbf{q})}. \quad (\text{P2})$$

Proof. Combine Lemma 3 with Proposition 1 applied to \mathcal{S}_D and the identity $\delta_{\mathcal{S}_D} = \delta^* + \beta_D$. For (P2), plug $\tau_{\mathcal{S}_D} = 1 - \delta_{\mathcal{S}_D} \geq 1 - \delta_{\varepsilon_D} = 1 - \delta^* - 2\varepsilon_D$ into (U2). \square

a) Token-Dropping Oracle (TDO): TDO generally uses posterior statistics (e.g., age, cumulative attention), so it naturally confines to (P1). Since the statistics may not be strictly relevant to the current \mathbf{q} , the surrogate error $\varepsilon_D(\mathbf{q})$ can be large when attention patterns shift, inflating the bias $2\varepsilon_D$.

b) *Query-Aware Approximation (QAA)*: QAA builds a query-conditioned compressed representation $B = B(\mathbf{K} | \mathbf{q}, C)$ (e.g., low-rank/sketch/ANN) that approximates oracle scores based on condition C . Let $\hat{A}_{\text{QAA}}(\mathbf{q})$ be the surrogate. Assume logit approximation with the supremum norm $\|\cdot\|_\infty$ is

$$\|a(\mathbf{q}) - \hat{a}(\mathbf{q})\|_\infty \leq \eta_C(\mathbf{q}), \quad a_i(q) = \mathbf{q}^\top \mathbf{k}_i / \sqrt{d}. \quad (\text{LogitError})$$

Lemma 4 (Softmax Lipschitz from logits to probabilities). *For any $a, \hat{a} \in \mathbb{R}^L$, $\|\text{softmax}(a) - \text{softmax}(\hat{a})\|_1 \leq 2 \|a - \hat{a}\|_\infty$.*

Proof. By the mean-value theorem, $\text{softmax}(\hat{a}) - \text{softmax}(a) = \left(\int_0^1 J(a + t(\hat{a} - a)) dt \right) (\hat{a} - a)$, where J is the softmax Jacobian with row $\nabla s_i = s_i(\mathbf{e}_i - s)$. One checks $\|J\|_{1 \rightarrow 1} \leq 2$ (each column sums to at most $2 \max_i s_i(1 - s_i) \leq 1/2$ in absolute value and the operator norm is attained by a signed vector; the resulting tight constant is 2), hence the claim holds. \square

Therefore,

$$\begin{aligned} \varepsilon_{\text{QAA}}(\mathbf{q}) &= \frac{1}{2} \|\hat{A}_{\text{QAA}}(\mathbf{q}) - A(\mathbf{q})\|_1 \\ &\leq \|a(\mathbf{q}) - \hat{a}(\mathbf{q})\|_\infty \leq \eta_C(\mathbf{q}). \end{aligned} \quad (\text{QAA-eps})$$

Let $\delta_\eta(\mathbf{q}) = \delta^*(\mathbf{q}) + 2\eta_C(\mathbf{q})$, Theorem 4 yields

$$I_{\text{full}}(q) - I_{\text{QAA}}(q) \leq 2[h_b(\delta_\eta(\mathbf{q})) + (\delta_\eta(\mathbf{q})) \log L]. \quad (\text{QAA})$$

Compare two post-hoc sparsity methods, since $\eta_C(q)$ can be made small with adequate compression rank/index quality, QAA typically incurs a *smaller* posterior bias than TDO.

C. Pre-hoc sparsity

Definition 1 (Pre-hoc selector with controlled mass error). *A pre-hoc selector $\mathcal{S}_{\text{pre}}(\mathbf{K}, \mathbf{q}; \zeta)$ (possibly using an theoretical error term ζ) is said to have mass error $\beta_{\text{th}}(\mathbf{q}) \geq 0$ if*

$$\begin{aligned} \tau_{\text{pre}}(\mathbf{q}) &\stackrel{\text{def}}{=} \sum_{i \in \mathcal{S}_{\text{pre}}(\mathbf{q})} A_i(\mathbf{q}) \geq \tau^*(\mathbf{q}) - \beta_{\text{th}}(\mathbf{q}), \\ \text{equivalently } \delta_{\text{pre}}(\mathbf{q}) &\leq \delta^*(\mathbf{q}) + \beta_{\text{th}}(\mathbf{q}), \end{aligned} \quad (30)$$

where $\tau^*(\mathbf{q})$ and $\delta^*(\mathbf{q})$ denote the oracle retained and dropped mass as stated in (20). We use either a pointwise control $\beta_{\text{th}}(\mathbf{q}) \leq \varepsilon_{\text{th}}$ a.s., or an average control $\mathbb{E}_q[\beta_{\text{th}}(\mathbf{q})] \leq \bar{\varepsilon}_{\text{th}}$, with $\varepsilon_{\text{th}}, \bar{\varepsilon}_{\text{th}} \ll 1$ to constrain ζ .

Theorem 5 (Information bound for pre-hoc). *For every query q , let $\delta_{\beta_{\text{th}}}(\mathbf{q}) = \delta^*(\mathbf{q}) + \beta_{\text{th}}(\mathbf{q})$,*

$$I_{\text{full}}(\mathbf{q}) - I_{\text{pre}}(\mathbf{q}) \leq 2[h_b(\delta_{\beta_{\text{th}}}(\mathbf{q})) + \delta_{\beta_{\text{th}}}(\mathbf{q}) \log L]. \quad (31)$$

Consequently, under the pointwise control $\beta_{\text{th}}(\mathbf{q}) \leq \varepsilon_{\text{th}}$,

$$\begin{aligned} I_{\text{full}}(\mathbf{q}) - I_{\text{pre}}(\mathbf{q}) \\ \leq 2[h_b(\delta^*(\mathbf{q}) + \varepsilon_{\text{th}}) + (\delta^*(\mathbf{q}) + \varepsilon_{\text{th}}) \log L]. \end{aligned} \quad (32)$$

Averaging over the query distribution and using $\mathbb{E}[\beta_{\text{th}}] \leq \bar{\varepsilon}_{\text{th}}$,

$$\begin{aligned} \mathbb{E}_{\mathbf{q}}[I_{\text{full}}(\mathbf{q}) - I_{\text{pre}}(\mathbf{q})] \\ \leq 2[h_b(\mathbb{E}_{\mathbf{q}}[\delta^*(\mathbf{q})] + \bar{\varepsilon}_{\text{th}}) + (\mathbb{E}_{\mathbf{q}}[\delta^*(\mathbf{q})] + \bar{\varepsilon}_{\text{th}}) \log L], \end{aligned} \quad (33)$$

where Jensen's inequality for the concave h_b is used. Moreover, the KL-based variant holds pointwise:

$$I_{\text{pre}}(\mathbf{q}) \geq I_{\text{full}}(\mathbf{q}) - \log \frac{1}{1 - \delta^*(\mathbf{q}) - \beta_{\text{th}}(\mathbf{q})}. \quad (34)$$

Proof. By Definition 1,

$$\delta_{\text{pre}}(\mathbf{q}) = 1 - \tau_{\text{pre}}(\mathbf{q}) \leq 1 - (\tau^*(\mathbf{q}) - \beta_{\text{th}}(\mathbf{q})) = \delta^*(\mathbf{q}) + \beta_{\text{th}}(\mathbf{q}).$$

Apply the universal continuity bound for any selector (**Proposition (U1)**) with δ_S replaced by $\delta_{\text{pre}}(\mathbf{q})$:

$$\begin{aligned} I_{\text{full}}(\mathbf{q}) - I_{\text{pre}}(\mathbf{q}) &\leq 2[h_b(\delta_{\text{pre}}(\mathbf{q})) + \delta_{\text{pre}}(\mathbf{q}) \log L] \\ &\leq 2[h_b(\delta^*(\mathbf{q}) + \beta_{\text{th}}(\mathbf{q})) + (\delta^*(\mathbf{q}) + \beta_{\text{th}}(\mathbf{q})) \log L], \end{aligned}$$

which is (31). The uniform version (32) follows by substituting $\beta_{\text{th}}(\mathbf{q}) \leq \varepsilon_{\text{th}}$. For the expectation bound (33), take expectations of the right-Hand side of (31), we use linearity for the $\log L$ term and Jensen's inequality $\mathbb{E}[h_b(\mathbf{X})] \leq h_b(\mathbb{E}[\mathbf{X}])$ for concave h_b . Finally, the KL variant (34) is the direct specialization of (U2) with $\tau_{\text{pre}}(\mathbf{q}) \geq 1 - \delta^*(\mathbf{q}) - \beta_{\text{th}}(\mathbf{q})$. \square

From the perspective of error expansion, let $g(\delta) = 2(h_b(\delta) + \delta \log L)$. For fixed $\delta^*(\mathbf{q})$ and small $\beta_{\text{th}}(\mathbf{q})$, a first-order Taylor expansion gives

$$\begin{aligned} g(\delta^*(\mathbf{q}) + \beta_{\text{th}}(\mathbf{q})) &= g(\delta^*(\mathbf{q})) + \\ &2\left(\log \frac{1 - \delta^*(\mathbf{q})}{\delta^*(\mathbf{q})} + \log L\right)\beta_{\text{th}}(\mathbf{q}) + \alpha(\beta_{\text{th}}(\mathbf{q})), \end{aligned}$$

so the additional loss induced by the theoretical error is approximately linear in $\beta_{\text{th}}(\mathbf{q})$ with slope $2 \log\left(\frac{L(1-\delta^*)}{\delta^*}\right)$. As $\beta_{\text{th}} \rightarrow 0$ we recover the original pre-hoc/oracle bound (with $\beta_{\text{th}} \equiv 0$).

Therefore, when the theoretical error is sufficiently small, our proposed pre-hoc sparsity approach demonstrates a definitive performance advantage over post-hoc sparsity methods.

REFERENCES

- [1] A. Hurst, A. Lerer, A. P. Goucher, A. Perelman, A. Ramesh, A. Clark, A. Ostrow, A. Welihinda, A. Hayes, A. Radford *et al.*, "Gpt-4o system card," *arXiv preprint arXiv:2410.21276*, 2024.
- [2] A. Liu, B. Feng, B. Xue, B. Wang, B. Wu, C. Lu, C. Zhao, C. Deng, C. Zhang, C. Ruan *et al.*, "Deepseek-v3 technical report," *arXiv preprint arXiv:2412.19437*, 2024.
- [3] Z. Wang, T. Luo, C. Liu, W. Liu, R. S. M. Goh, and W.-F. Wong, "Enabling energy-efficient deployment of large language models on memristor crossbar: A synergy of large and small," *IEEE Transactions on Pattern Analysis and Machine Intelligence*, vol. 47, no. 2, pp. 916–933, 2025.
- [4] Z. Yi, J. Ouyang, Z. Xu, Y. Liu, T. Liao, H. Luo, and Y. Shen, "A survey on recent advances in llm-based multi-turn dialogue systems," *ACM Comput. Surv.*, 2025.
- [5] Z. Teng, Y. Song, X. Ye, and Y. Ouyang, "Fine-tuning llms for multi-turn dialogues: optimizing cross-entropy loss with kl divergence for all rounds of responses," in *Proceedings of the 2024 16th International Conference on Machine Learning and Computing*, 2024, pp. 128–133.

- [6] Z.-A. Ma, T. Lan, R.-C. Tu, Y. Hu, Y.-S. Zhu, T. Zhang, H. Huang, Z. Wu, and X.-L. Mao, "Multi-modal retrieval augmented multi-modal generation: Datasets, evaluation metrics and strong baselines," *arXiv preprint arXiv:2411.16365*, 2024.
- [7] Z. Zhang, H. Elfardy, M. Dreyer, K. Small, H. Ji, and M. Bansal, "Enhancing multi-document summarization with cross-document graph-based information extraction," in *Proceedings of the 17th Conference of the European Chapter of the Association for Computational Linguistics*, 2023, pp. 1696–1707.
- [8] Y. Liu, K. Shi, K. He, L. Ye, A. Fabbri, P. Liu, D. Radev, and A. Cohan, "On learning to summarize with large language models as references," in *Proceedings of the 2024 Conference of the North American Chapter of the Association for Computational Linguistics: Human Language Technologies (Volume 1: Long Papers)*, Jun. 2024, pp. 8647–8664.
- [9] R.-C. Tu, X.-L. Mao, K. Q. Lin, C. Cai, W. Qin, W. Wei, H. Wang, and H. Huang, "Unsupervised hashing with semantic concept mining," *Proceedings of the ACM on Management of Data*, vol. 1, no. 1, pp. 1–19, 2023.
- [10] H. Liu, C. Li, Q. Wu, and Y. J. Lee, "Visual instruction tuning," *Advances in Neural Information Processing Systems*, vol. 36, pp. 34 892–34 916, 2023.
- [11] B. Lin, Y. Ye, B. Zhu, J. Cui, M. Ning, P. Jin, and L. Yuan, "Video-LLaVA: Learning united visual representation by alignment before projection," in *Proceedings of the 2024 Conference on Empirical Methods in Natural Language Processing*, Miami, Florida, USA, Nov. 2024, pp. 5971–5984.
- [12] R.-C. Tu, Y. Ji, J. Jiang, W. Kong, C. Cai, W. Zhao, H. Wang, Y. Yang, and W. Liu, "Global and local semantic completion learning for vision-language pre-training," *IEEE Transactions on Pattern Analysis and Machine Intelligence*, 2025.
- [13] Z. Qin, D. Chen, W. Zhang, L. Yao, Y. Huang, B. Ding, Y. Li, and S. Deng, "The synergy between data and multi-modal large language models: A survey from co-development perspective," *IEEE Transactions on Pattern Analysis and Machine Intelligence*, pp. 1–20, 2025.
- [14] R.-C. Tu, Z.-A. Ma, T. Lan, Y. Zhao, H.-Y. Huang, and X.-L. Mao, "Automatic evaluation for text-to-image generation: Task-decomposed framework, distilled training, and meta-evaluation benchmark," in *Proceedings of the 63rd Annual Meeting of the Association for Computational Linguistics (Volume 1: Long Papers)*, 2025, pp. 22 340–22 361.
- [15] Z. Yu, X. Ouyang, Z. Shao, M. Wang, and J. Yu, "Prophet: Prompting large language models with complementary answer heuristics for knowledge-based visual question answering," *IEEE Transactions on Pattern Analysis and Machine Intelligence*, pp. 1–12, 2025.
- [16] Z. Huang, S. Zhong, P. Zhou, S. Gao, M. Zitnik, and L. Lin, "A causality-aware paradigm for evaluating creativity of multimodal large language models," *IEEE Transactions on Pattern Analysis and Machine Intelligence*, vol. 47, no. 5, pp. 3830–3846, 2025.
- [17] R.-C. Tu, W. Sun, H. You, Y. Wang, J. Huang, L. Shen, and D. Tao, "Multimodal reasoning agent for zero-shot composed image retrieval," *arXiv preprint arXiv:2505.19952*, 2025.
- [18] F. Liu, X. Wu, J. Huang, B. Yang, K. Branson, P. Schwab, L. Clifton, P. Zhang, J. Luo, Y. Zheng, and D. A. Clifton, "Aligning, autoencoding and prompting large language models for novel disease reporting," *IEEE Transactions on Pattern Analysis and Machine Intelligence*, vol. 47, no. 5, pp. 3332–3343, 2025.
- [19] T. Lan, Y.-H. Zhou, Z.-A. Ma, F. Sun, R.-Q. Sun, J. Luo, R.-C. Tu, H. Huang, C. Xu, Z. Wu *et al.*, "A survey of automatic evaluation methods on text, visual and speech generations," *arXiv preprint arXiv:2506.10019*, 2025.
- [20] R.-C. Tu, Z. Jin, J. Liao, X. Luo, Y. Wang, L. Shen, and D. Tao, "Mllm-guided vlm fine-tuning with joint inference for zero-shot composed image retrieval," *arXiv preprint arXiv:2505.19707*, 2025.
- [21] A. Vaswani, N. Shazeer, N. Parmar, J. Uszkoreit, L. Jones, A. N. Gomez, Ł. Kaiser, and I. Polosukhin, "Attention is all you need," *Advances in Neural Information Processing Systems*, vol. 30, 2017.
- [22] H. Touvron, T. Lavril, G. Izacard, X. Martinet, M.-A. Lachaux, T. Lacroix, B. Rozière, N. Goyal, E. Hambro, F. Azhar *et al.*, "Llama: Open and efficient foundation language models," *arXiv preprint arXiv:2302.13971*, 2023.
- [23] S. Wang, B. Z. Li, M. Khabsa, H. Fang, and H. Ma, "Linformer: Self-attention with linear complexity," *arXiv preprint arXiv:2006.04768*, 2020.
- [24] W. Sun, R.-C. Tu, Y. Ding, Z. Jin, J. Liao, S. Liu, and D. Tao, "Vorta: Efficient video diffusion via routing sparse attention," *arXiv preprint arXiv:2505.18809*, 2025.
- [25] Z. Zhang, Y. Sheng, T. Zhou, T. Chen, L. Zheng, R. Cai, Z. Song, Y. Tian, C. Ré, C. Barrett *et al.*, "H2o: Heavy-hitter oracle for efficient generative inference of large language models," *Advances in Neural Information Processing Systems*, vol. 36, pp. 34 661–34 710, 2023.
- [26] G. Xiao, Y. Tian, B. Chen, S. Han, and M. Lewis, "Efficient streaming language models with attention sinks," in *The Twelfth International Conference on Learning Representations*, 2024.
- [27] Y. He, L. Zhang, W. Wu, J. Liu, H. Zhou, and B. Zhuang, "Zipcache: Accurate and efficient kv cache quantization with salient token identification," in *Advances in Neural Information Processing Systems*, vol. 37, 2024, pp. 68 287–68 307.
- [28] Z. Wan, X. Wu, Y. Zhang, Y. Xin, C. Tao, Z. Zhu, X. Wang, S. Luo, J. Xiong, L. Wang, and M. Zhang, "D2o: Dynamic discriminative operations for efficient long-context inference of large language models," in *The Thirteenth International Conference on Learning Representations*, 2025.
- [29] J. Tang, Y. Zhao, K. Zhu, G. Xiao, B. Kasikci, and S. Han, "Quest: query-aware sparsity for efficient long-context LLM inference," in *Proceedings of the 41st International Conference on Machine Learning*, ser. ICML'24, 2024, pp. 47 901–47 911.
- [30] H. Sun, L.-W. Chang, W. Bao, S. Zheng, N. Zheng,

- X. Liu, and et al., “ShadowKV: KV cache in shadows for high-throughput long-context LLM inference,” in *Proceedings of the 42nd International Conference on Machine Learning*, 2025, pp. 57 355–57 373.
- [31] W. Wu, Z. Pan, K. Fu, C. Wang, L. Chen, Y. Bai, and at al., “TokenSelect: Efficient long-context inference and length extrapolation for LLMs via dynamic token-level KV cache selection,” in *Proceedings of the 2025 Conference on Empirical Methods in Natural Language Processing*, 2025, pp. 21 275–21 292.
- [32] M. Liu, T. Rabbani, T. O’Halloran, A. Sankaralingam, M.-A. Hartley, B. Gravelle, F. Huang, C. Fermüller, and Y. Aloimonos, “Hashevict: A pre-attention kv cache eviction strategy using locality-sensitive hashing,” *arXiv preprint arXiv:2412.16187*, 2024.
- [33] H. Wu, L. Li, H. Huang, T. Yi, J. Zhang, M. Yu, and J. Yan, “HShare: Fast LLM decoding by hierarchical key-value sharing,” in *The Thirteenth International Conference on Learning Representations*, 2025.
- [34] A. Liu, J. Liu, Z. Pan, Y. He, G. Haffari, and B. Zhuang, “Minicache: Kv cache compression in depth dimension for large language models,” in *Proceedings of the 38th International Conference on Neural Information Processing Systems*, 2025, pp. 139 997–140 031.
- [35] A. Q. Jiang, A. Sablayrolles, A. Mensch, C. Bamford, D. S. Chaplot, D. de las Casas, F. Bressand, G. Lengyel, G. Lample, L. Saulnier, L. R. Lavaud, M.-A. Lachaux, P. Stock, T. L. Scao, T. Lavril, T. Wang, T. Lacroix, and W. E. Sayed, “Mistral 7b,” 2023. [Online]. Available: <https://arxiv.org/abs/2310.06825>
- [36] M. Ott, S. Edunov, A. Baevski, A. Fan, S. Gross, N. Ng, D. Grangier, and M. Auli, “fairseq: A fast, extensible toolkit for sequence modeling,” in *Proceedings of the 2019 Conference of the North American Chapter of the Association for Computational Linguistics (Demonstrations)*, Jun. 2019, pp. 48–53.
- [37] G. Xiao, J. Tang, J. Zuo, J. Guo, S. Yang, H. Tang, Y. Fu, and S. Han, “Duoattention: Efficient long-context LLM inference with retrieval and streaming heads,” in *The Thirteenth International Conference on Learning Representations*, 2025.
- [38] G. Liu, C. Li, Z. Ning, J. Lin, Y. Yao, D. Ke, M. Guo, and J. Zhao, “Freekv: Boosting kv cache retrieval for efficient llm inference,” *arXiv*, 2025.
- [39] Y. Li, Y. Huang, B. Yang, B. Venkitesh, A. Locatelli, H. Ye, T. Cai, P. Lewis, and D. Chen, “Snapkv: Llm knows what you are looking for before generation,” *Advances in Neural Information Processing Systems*, vol. 37, pp. 22 947–22 970, 2024.
- [40] S. Ge, Y. Zhang, L. Liu, M. Zhang, J. Han, and J. Gao, “Model tells you what to discard: Adaptive KV cache compression for LLMs,” in *The Twelfth International Conference on Learning Representations*, 2024.
- [41] Z. Cai, Y. Zhang, B. Gao, Y. Liu, Y. Li, T. Liu, and at al., “PyramidKV: Dynamic KV cache compression based on pyramidal information funneling,” in *Second Conference on Language Modeling*, 2025.
- [42] Y. Gao, L. Wang, J. Fang, L. Hu, and J. Cheng, “Empower your model with longer and better context comprehension,” *arXiv*, 2023.
- [43] J. Su, M. Ahmed, Y. Lu, S. Pan, W. Bo, and Y. Liu, “Roformer: Enhanced transformer with rotary position embedding,” *Neurocomputing*, vol. 568, p. 127063, 2024.
- [44] S. Yang, Y. Sheng, J. E. Gonzalez, I. Stoica, and L. Zheng, “Post-training sparse attention with double sparsity,” *arXiv preprint arXiv:2408.07092*, 2024.
- [45] K. Cobbe, V. Kosaraju, M. Bavarian, M. Chen, H. Jun, L. Kaiser, M. Plappert, J. Tworek, J. Hilton, R. Nakano *et al.*, “Training verifiers to solve math word problems,” *arXiv preprint arXiv:2110.14168*, 2021.
- [46] S. Reddy, D. Chen, and C. D. Manning, “Coqa: A conversational question answering challenge,” *Transactions of the Association for Computational Linguistics*, vol. 7, pp. 249–266, 2019.
- [47] Y. Bai, X. Lv, J. Zhang, H. Lyu, J. Tang, Z. Huang, Z. Du, X. Liu, A. Zeng, L. Hou, Y. Dong, J. Tang, and J. Li, “LongBench: A bilingual, multitask benchmark for long context understanding,” in *Proceedings of the 62nd Annual Meeting of the Association for Computational Linguistics (Volume 1: Long Papers)*, Aug. 2024, pp. 3119–3137.
- [48] T. Dao, D. Fu, S. Ermon, A. Rudra, and C. Ré, “Flashattention: Fast and memory-efficient exact attention with io-awareness,” *Advances in neural information processing systems*, vol. 35, pp. 16 344–16 359, 2022.
- [49] PyTorch Team, “Accelerating generative ai with pytorch 2.0,” <https://pytorch.org/blog/pytorch-2/>, 2023.
- [50] Z. Liu, J. Wang, T. Dao, T. Zhou, B. Yuan, Z. Song, A. Shrivastava, C. Zhang, Y. Tian, C. Re *et al.*, “Deja vu: Contextual sparsity for efficient llms at inference time,” in *International Conference on Machine Learning*, 2023, pp. 22 137–22 176.



Yifei Gao is pursuing the master degree at University College London. He previously obtained his B.Eng. degree from the College of Software Engineering at the University of Electronic Science and Technology of China in 2024. His current research interests encompass large language models, 3D reconstruction, and diffusion models.



Lei Wang (Senior Member, IEEE) received the Ph.D. degree in Electrical Engineering from Xidian University, Xi’an, China, in 2010. From 2011 to 2012, he was with Huawei Technologies Company Ltd. From 2014 to 2015, he was with the Department of Embedded Systems Engineering, Incheon National University, as a Postdoctoral Fellow. He is currently an Associate Professor with the Shenzhen Institutes of Advanced Technology, Chinese Academy of Sciences, Shenzhen, China. He has authored or coauthored more than 70 papers in conferences and journals, including IEEE TRANSACTIONS ON CIRCUITS AND SYSTEMS FOR VIDEO TECHNOLOGY, IEEE TRANSACTIONS ON CYBERNETICS, IEEE TRANSACTIONS ON MULTIMEDIA, IEEE SIGNAL PROCESSING LETTERS, and NAACL. His research interests include image processing, transforms, machine learning, computer vision, 3-D reconstruction, and robotics.



Rong-Cheng Tu received the B.S. degree in 2018 and the Ph.D. degree in 2023 from the Beijing Institute of Technology, Beijing, China. He is currently a Research Fellow with Nanyang Technological University (NTU), Singapore. His research interests include deep learning, information retrieval, and Large Language Model efficiency.



Qixin Zhang received his B.S. degree from the University of Science and Technology of China in 2018. He subsequently earned his Ph.D. degree in the School of Data Science at City University of Hong Kong in 2024. Currently, he is a Research Fellow at Nanyang Technological University, Singapore. His research interests include submodular optimization, subset selection and network prune. He has published over 15 papers in top data science venues such as ICML, NeurIPS, ICLR, AISTATS, AAAI and TKDE, etc.



Jun Cheng (Senior Member, IEEE) received the B.Eng. and M.Eng. degrees from the University of Science and Technology of China, Hefei, China, in 1999 and 2002, respectively, and the Ph.D. degree from Chinese University of Hong Kong, Hong Kong, in 2006. He is currently a Professor with Shenzhen Institutes of Advanced Technology, Chinese Academy of Sciences, Shenzhen, China, where he is also the Director of the Laboratory for Human Machine Control. His current research interests include computer vision, robotics, machine intelligence, and control.



Dacheng Tao (F'15) is currently a Distinguished University Professor in the College of Computing & Data Science at Nanyang Technological University. He mainly applies statistics and mathematics to artificial intelligence and data science, and his research is detailed in one monograph and over 200 publications in prestigious journals and proceedings at leading conferences, with best paper awards, best student paper awards, and test-of-time awards. His publications have been cited over 126K times and he has an hindex 160+ in Google Scholar. He received

the 2015 and 2020 Australian Eureka Prize, the 2018 IEEE ICDM Research Contributions Award, and the 2021 IEEE Computer Society McCluskey Technical Achievement Award. He is a Fellow of the Australian Academy of Science, AAAS, ACM and IEEE.

APPENDIX

A. Mean-shift Property of Token-sparse Attention

In this section, building upon prior research Deja Vu [50], we first describe the analytical foundation of our work: self-attention can be interpreted as a form of mean-shift clustering. Based on this perspective, we then explore the among-query properties of self-attention and leveraging the formal definition of TSA (as introduced in **Definition 3.1**) to construct and complete our theoretical proof.

1) Self-Attention as Mean-Shift Clustering:

a) *Implicit Clustering in Attention*: The softmax weighting means that the query \mathbf{q} mainly focuses on a subset of keys with the largest dot-products $\mathbf{q} \cdot \mathbf{k}_j$. This behavior causes tokens to form clusters: tokens (keys) that are similar to a given query will receive high attention weights (“cluster members”), whereas unrelated tokens get negligible weight. In other words, each query **picks out clusters** of relevant key tokens and largely ignores the rest, which is exactly the token sparsity phenomenon [25, 29] (only a few tokens significantly contribute to the attention result).

b) *Mean-Shift Interpretation*: Importantly, the Deja Vu study observed that **self-attention implements a one-step mean-shift clustering update**. Formally, fixing within one head, for the attention output $\mathbf{y} = \sum_i A_i(\mathbf{x}_i \mathbf{W}_V)$, if we ignore the \mathbf{W}_V projection for a moment, this computes the *weighted centroid* of the token embeddings \mathbf{x} around the query \mathbf{q} (in the projected space). That is, define an *attention mean* $m(\mathbf{q})$ as the weighted mean of the embeddings:

$$m(\mathbf{q}) = \frac{\sum_i \mathbf{K}(\mathbf{x}_i, \mathbf{q}) \mathbf{x}_i}{\sum_i \mathbf{K}(\mathbf{x}_i, \mathbf{q})}, \quad (35)$$

so $\mathbf{y} = m(\mathbf{q}) \mathbf{W}_V$. This is exactly the update step of the **mean-shift clustering algorithm**: $m(\mathbf{q})$ is pulling the query’s embedding toward a nearby cluster of points \mathbf{x}_i that are similar to \mathbf{q} . In mean-shift, one would iteratively set $\mathbf{q} \leftarrow m(\mathbf{q})$ to converge to the cluster center (mode of the density). In a Transformer, we usually apply just one such step per layer, but the analogy holds: *each attention head nudges the query vector toward the centroid of a cluster of key vectors*.

2) Among-Query Property:

a) *Problem Setting*: Consider two queries \mathbf{q}_t and \mathbf{q}_{t+1} from adjacent time steps in a sequence. Thanks to residual connections and the smooth nature of transformer dynamics, adjacent queries in a sequence tend to be close in embedding space [30, 33]. We then assume as a general principle that \mathbf{q}_{t+1} is a *small perturbation* of \mathbf{q}_t (i.e. $\mathbf{q}_{t+1} \approx \mathbf{q}_t$ in ℓ_2 norm or cosine similarity), as the among-query property only concerns the behavior of attention when queries are similar, we revise the **Among-query Property 1** that:

Property 2 (Among-query Property). *If two query vectors \mathbf{q}_t and \mathbf{q}_{t+1} are aligned enough in vector space, then the distributions of their attention weights are also very similar.*

In other words, adjacent queries attend to largely the same cluster of key tokens. As \mathbf{q}_t shifts to \mathbf{q}_{t+1} , the attention weight mass simply shifts smoothly among those keys—obeying a continuous mean-shift-like change—rather than jumping to a completely different set of keys.

b) *Intuition via Mean-Shift*: Think of the keys \mathbf{k}_i as data points in the embedding space. The query \mathbf{q}_t will put most weight on keys in some neighborhood (a “cluster”) around \mathbf{q}_t . Now if \mathbf{q}_{t+1} moves slightly (say $\mathbf{q}_{t+1} = \mathbf{q}_t + \Delta$ for a small Δ), it will still lie in roughly the same neighborhood of points. The attention kernel $\mathbf{K}(x_i, \mathbf{q}) = \exp(\mathbf{q} \cdot \mathbf{k}_i)$ is a smooth, continuous function of q . A slight change in \mathbf{q} causes only a slight change in all the similarity scores $\mathbf{q} \cdot \mathbf{k}_i$. Thus the weights A_i shift slightly: keys that are highly ranked for \mathbf{q}_t will remain highly ranked for \mathbf{q}_{t+1} , as long as \mathbf{q}_{t+1} hasn’t moved so far that it finds a totally different cluster.

c) *Formal Derivation of the Among-Query Property*: Let $\mathbf{K} = \{\mathbf{k}_1, \mathbf{k}_2, \dots, \mathbf{k}_t\}$ be the key vectors available. Consider two queries \mathbf{q} and \mathbf{q}' (think of $\mathbf{q} = \mathbf{q}_t$ and $\mathbf{q}' = \mathbf{q}_{t+1}$) such that \mathbf{q}' is a small perturbation of \mathbf{q} . We will show that the attention distributions of $A(\mathbf{q})$ and $A(\mathbf{q}')$ are *close*, and in particular that the high-weight components of $A(\mathbf{q})$ correspond to high-weight components of $A(\mathbf{q}')$. We also look at the weighted average outputs $\mathbf{y}(\mathbf{q})$ and $\mathbf{y}(\mathbf{q}')$. We first consider the perturbation changes in queries (e.g., \mathbf{q} to \mathbf{q}') to that of logits. For each key \mathbf{k}_i , the score (logit) for q as $a_i = \frac{1}{\sqrt{d}} \mathbf{q} \cdot \mathbf{k}_i$ and for \mathbf{q}' as $a'_i = \frac{1}{\sqrt{d}} \mathbf{q}' \cdot \mathbf{k}_i$. Because $\mathbf{q}' = \mathbf{q} + \Delta$ for a small Δ , we have $a'_j - a_j = \frac{1}{\sqrt{d}} (\mathbf{q}' - \mathbf{q}) \cdot \mathbf{k}_j = \frac{1}{\sqrt{d}} \Delta \cdot \mathbf{k}_j$.

Let $\Delta_i := a'_i - a_i$. Since $|\Delta|$ is small and (typically) the keys \mathbf{k}_i have bounded norm, each Δ_i is a small real number. In other words, the entire vector of logits $a' = (a'_1, \dots, a'_t)$ is a small perturbation of $a = (a_1, \dots, a_t)$, and there exists some $\epsilon \ll 1$ such that $|\Delta_i| \leq \epsilon$ for all i . (Δ_i might vary across i , but we can bound the maximum change by $\epsilon = \frac{|\Delta| \max_i |\mathbf{k}_i|}{\sqrt{d}}$.) Then, combining the Softmax part in attention weights, by definition, $A_j(\mathbf{q}) = \frac{e^{a_j}}{\sum_j e^{a_j}}$ and $A_j(\mathbf{q}') = \frac{e^{a'_j}}{\sum_j e^{a'_j}}$. It will be convenient to express $A_i(\mathbf{q}')$ in terms of $A(\mathbf{q})$ and the perturbations Δ_i . We can write:

$$A_i(\mathbf{q}') = \frac{e^{a_i + \Delta_i}}{\sum_j e^{z_j + \Delta_j}} = \frac{e^{z_i} e^{\Delta_i}}{\sum_j e^{z_j} e^{\Delta_j}} = \frac{A_j(\mathbf{q}) e^{\Delta_i}}{\sum_j A_j(\mathbf{q}) e^{\Delta_j}}. \quad (36)$$

Here we use $e^{a_i} / \sum_j e^{a_j} = A_i(\mathbf{q})$ and factored e^{Δ_j} out of the denominator. Let $A^n = \sum_j A_j(\mathbf{q}) e^{\Delta_j}$ denote the normalization factor that adjusts the weights due to the query change. Since each Δ_j is small, we can expand A^n in a Taylor series:

$$A^n = \sum_j A_j(\mathbf{q}) (1 + \Delta_j + O(\Delta_j^2)) = 1 + \sum_j A_j(\mathbf{q}) \Delta_j + O(\epsilon^2). \quad (37)$$

Here $\sum_j A_j(\mathbf{q}) \Delta_j$ is the expectation of Δ under the original distribution $A(\mathbf{q})$. Let $\mu_\Delta = \sum_j A_j(\mathbf{q}) \Delta_j$ for brevity. Combining Eq. (37), we can write $A^n = 1 + \mu_\Delta + O(\epsilon^2)$. Using this, we can approximate the new weights $A_i(\mathbf{q}')$ based on the First-Order Taylor Approximation in small Δ ,

$$A_i(\mathbf{q}') \approx \frac{A_i(\mathbf{q})(1 + \Delta_i)}{1 + \mu_\Delta} \approx A_i(\mathbf{q})(1 + \Delta_i - \mu_\Delta), \quad (38)$$

where second approximation used $\frac{1}{1 + \mu_\Delta} \approx 1 - \mu_\Delta$ for small μ_Δ . Thus, for small query shifts, the new attention weight is approximately $A_i(\mathbf{q}') \approx A_i(\mathbf{q}) + A_i(\mathbf{q})(\Delta_i - \mu_\Delta)$. This formula reveals how the attention distribution shifts in response to Δ :

- If Δ_i is larger than the average μ_Δ , then A_i will increase ($\Delta_i - \mu_\Delta > 0$).
- If Δ_i is smaller than the average, A_i will decrease slightly.
- The total change is zero-sum to first order as shown in Eq. (39), as expected (the weights still sum to 1).

$$\begin{aligned} \sum_i [A_i(\mathbf{q}') - A_i(\mathbf{q})] &\approx \sum_i A_i(\mathbf{q})(\Delta_i - \mu_\Delta) \\ &= (\sum_i A_i(\mathbf{q})\Delta_i) - \mu_\Delta \sum_i A_i(\mathbf{q}) = \mu_\Delta - \mu_\Delta(1) = 0 \end{aligned} \quad (39)$$

d) *Transmission to Token-sparse Attention*: After proving the minimal attention score shifts in self-attention, we integrate them to the token-sparse attention defined in Sec. II-B. Suppose the original query \mathbf{q} had a set of critical keys (a cluster) $C = \{i : A_i(\mathbf{q})\}$ is among the top weights and above some importance threshold. We want to show that for \mathbf{q}' , the high-weight keys $C' = \{i : A_i(\mathbf{q}')\}$ largely overlap with C . From the approximation above, if $i \in C$ had a large original weight $A_i(\mathbf{q})$, then $A_i(\mathbf{q}')$ will remain large unless something drastic happens to Δ_i , as $\mathbf{q}' \cdot \mathbf{k}_i$ will remain relatively larger for those same $i \in C$ than for others.

For any i in the original top cluster C , a_i was high relative to most other a_j . The change Δ_i would have to be exceptionally negative (compared to others) to knock i out of the top ranks. But $\Delta_i = \frac{1}{\sqrt{d}} \Delta \cdot \mathbf{k}_i$ is small for all i , so it's highly unlikely to completely invert the ordering of scores. In effect, the ranking of the top few A_i is stable under small perturbations of \mathbf{q} . (One can make this rigorous by noting that softmax is a Lipschitz continuous function of its input logits; a sufficiently small change in \mathbf{q} cannot cause a large change in the output distribution. More concretely, if $|\Delta_i| < \delta$ for all j , then $\max_i |A_i(\mathbf{q}') - A_i(\mathbf{q})|$ is $O(\delta)$ and the indices of the top weights cannot all change at once.)

For any i outside the cluster ($i \notin C$ with tiny $A_i(\mathbf{q})$), \mathbf{q}' would have to move much closer to \mathbf{k}_i (relative to the others) to elevate its weight significantly. A small Δ won't make a previously irrelevant key suddenly important. Thus those outside keys remain with near-zero weight in $A(\mathbf{q}')$. These observations imply C' will contain C or at least have large overlap. **Overall, \mathbf{q} and \mathbf{q}' induce very similar attention weight distributions.** Quantitatively, one could bound the KL-divergence or total variation between $A(\mathbf{q})$ and $A(\mathbf{q}')$ in terms of $|\Delta|$. But the key point is that no single small Δ causes a big discrete jump in the distribution.

e) *Smooth Shift of the Attention Centroid*: Because the weight distribution shifts only slightly, the centroid (weighted average) of the attended keys also shifts smoothly. The output for query \mathbf{q}' is thus

$$\begin{aligned} \mathbf{y}(\mathbf{q}') &= \sum_i [A_i(\mathbf{q}) + A_i(\mathbf{q})(\Delta_i - \mu_\Delta)] \mathbf{k}_i \\ &\approx \sum_i A_i(\mathbf{q}) \mathbf{k}_i + \sum_i A_i(\mathbf{q})(\Delta_i - \mu_\Delta) \mathbf{k}_i. \end{aligned} \quad (40)$$

The second term is a small adjustment. In fact, note that $\sum_i A_i(\mathbf{q}) \Delta_i \mathbf{k}_i = (\Delta \cdot \mathbf{k}_i)$ weighted by A_i , this is roughly Δ projected onto the direction of the original output. Without going too deep into the algebra, the main result indicates that $\mathbf{y}(\mathbf{q}') - \mathbf{y}(\mathbf{q})$ is of order $O(|\Delta|)$, a small change. Geometrically,

if $\mathbf{y}(\mathbf{q})$ is (proportional to) the mean of cluster C , then $\mathbf{y}(\mathbf{q}')$ will be the mean of almost the same cluster, just adjusted towards \mathbf{q}' . **This is precisely what we expect from a mean-shift update: as the query moves, the cluster centroid moves along with it, continuously.**

3) *Centroid Shift*: We formalize the Lipschitz continuity of the attention centroid with respect to the query. Follow the definition in Sec. A2c, let $\{p_i\}_{i=1}^t \subset \mathbb{R}$ be scalar token positions (sequence coordinates), and define the sequence-axis centroid $c(\mathbf{q}) = \sum_{i=1}^t A_i(\mathbf{q}) p_i$. Assume unit-norm queries ($\|\mathbf{q}\| = \|\mathbf{q}'\| = 1$) so that $\|\mathbf{q}' - \mathbf{q}\| = \sqrt{2 - 2 \cos \angle(\mathbf{q}, \mathbf{q}')}$; non-normalized statements follow by the triangle inequality. We write $K_{\max} \stackrel{\text{def}}{=} \max_i \|\mathbf{k}_i\|$ and $\text{diam } \mathcal{P} = \max_i p_i - \min_i p_i$.

Lemma 5 (Softmax $\ell_\infty \rightarrow \ell_1$ Lipschitzness). *For any $a, a' \in \mathbb{R}^t$,*

$$\|\text{softmax}(a') - \text{softmax}(a)\|_1 \leq 2 \|a' - a\|_\infty.$$

Proof. By the mean value theorem on the line segment between a and a' , for some \tilde{a} we have $\text{softmax}(a') - \text{softmax}(a) = J(\tilde{a})(a' - a)$, where $J(\tilde{a}) = \text{diag}(A) - AA^\top$ is the Jacobian at \tilde{a} with $A = \text{softmax}(\tilde{a})$. One checks that $\|J(\tilde{a})\|_{\infty \rightarrow 1} \leq 2$ (equivalently, the total variation norm of the softmax is 2-Lipschitz with respect to ℓ_∞ perturbations of logits). Hence $\|\text{softmax}(a') - \text{softmax}(a)\|_1 \leq 2 \|a' - a\|_\infty$. \square

Lemma 6 (Logit change under query perturbation). *Let $\mathbf{q}' = \mathbf{q} + \Delta$. Then*

$$\|a(\mathbf{q}') - a(\mathbf{q})\|_\infty = \max_i \frac{1}{\sqrt{d}} |\Delta^\top \mathbf{k}_i| \leq \frac{K_{\max}}{\sqrt{d}} \|\Delta\|.$$

Proof. Immediate from Cauchy-Schwarz: $|\Delta^\top \mathbf{k}_i| \leq \|\Delta\| \|\mathbf{k}_i\|$. \square

Theorem 6 (Query-Lipschitz Centroid Drift). *For $\mathbf{q}' = \mathbf{q} + \Delta$,*

$$\begin{aligned} |c(\mathbf{q}') - c(\mathbf{q})| &\leq (\text{diam } \mathcal{P}) \cdot \|A(\mathbf{q}') - A(\mathbf{q})\|_1 \\ &\leq 2 (\text{diam } \mathcal{P}) \cdot \frac{K_{\max}}{\sqrt{d}} \|\Delta\|. \end{aligned} \quad (41)$$

In particular, $c(\mathbf{q}') = c(\mathbf{q}) + O(\|\Delta\|)$.

Proof. By definition, $|c(\mathbf{q}') - c(\mathbf{q})| \leq \|A(\mathbf{q}') - A(\mathbf{q})\|_1 \cdot \max_i |p_i - \bar{p}|$ for any \bar{p} . Choosing $\bar{p} \in [\min_i p_i, \max_i p_i]$ gives $\max_i |p_i - \bar{p}| \leq \text{diam } \mathcal{P}$, hence the first inequality. The second inequality follows by Lemmas 5 and 6. \square

4) *CIS MI Bound Parameterization*: We connect CIS parameters (τ, m, r) to the pre-hoc retained-mass gap β_{th} , which feeds into the MI bound in Eq. (4).

a) *Notation*: Fix a head and a decoding step t . Let $\mathcal{S}_t^*(\mathbf{q})$ be the oracle top- k set under query \mathbf{q} , sorted by attention weight. Let $\mathcal{S}_{t,m}(\mathbf{q}) \subset \mathcal{S}_t^*(\mathbf{q})$ be its top- m winners. For an integer radius $r \geq 0$, define the r -neighborhood (on the sequence axis) $\mathcal{N}_r(S) = \bigcup_{p \in S} \{p + \delta : \delta \in \{-r, \dots, r\}\}$ with clipping to $[1, t]$. CIS reuses $\hat{\mathcal{S}}_t(\mathbf{q}) \stackrel{\text{def}}{=} \mathcal{S}_t^*(\mathbf{q}) \cup \mathcal{N}_r(\mathcal{S}_{t,m}(\mathbf{q}))$. For a later query \mathbf{q}' in the same block with cosine similarity $\text{sim}(\mathbf{q}, \mathbf{q}') \geq \tau$, CIS uses $\hat{\mathcal{S}}_t(\mathbf{q})$ as the shared index set for \mathbf{q}' (per Eq. (13)). Define retained mass $\tau_{\hat{\mathcal{S}}_t}(\mathbf{q}) = \sum_{i \in \hat{\mathcal{S}}_t(\mathbf{q})} A_i(\mathbf{q})$ and $\tau_{\text{pre}}(\mathbf{q}') = \sum_{i \in \hat{\mathcal{S}}_t(\mathbf{q})} A_i(\mathbf{q}')$, and the oracle mass $\tau^*(\mathbf{q}') = \sum_{i \in \mathcal{S}_t^*(\mathbf{q}')} A_i(\mathbf{q}')$. Let $\Delta_{\text{att}}(\tau) = \|A(\mathbf{q}') - A(\mathbf{q})\|_1$.

Lemma 7 (Similarity \Rightarrow attention variation). *If $\|\mathbf{q}\|=\|\mathbf{q}'\|=1$ and $\text{sim}(\mathbf{q}, \mathbf{q}')=\cos \angle(\mathbf{q}, \mathbf{q}') \geq \tau$, then*

$$\Delta_{\text{att}}(\tau) \leq \frac{2K_{\max}}{\sqrt{d}} \|\mathbf{q}' - \mathbf{q}\| = \frac{2K_{\max}}{\sqrt{d}} \sqrt{2-2\tau}.$$

Proof. Combine Lemmas 5–6 and $\|\mathbf{q}' - \mathbf{q}\| = \sqrt{2-2\tau}$ for unit-norm queries. \square

Lemma 8 (Oracle continuity). $|\tau^*(\mathbf{q}') - \tau^*(\mathbf{q})| \leq \Delta_{\text{att}}(\tau)$.

Proof. For any fixed index set S , the map $q \mapsto \sum_{i \in S} A_i(\mathbf{q})$ is 1-Lipschitz in total variation: $|\sum_{i \in S} (A_i(\mathbf{q}') - A_i(\mathbf{q}))| \leq \|A(\mathbf{q}') - A(\mathbf{q})\|_1$. Taking $S = \mathcal{S}_t^*(\mathbf{q}')$ yields $\tau^*(\mathbf{q}') \leq \sum_{i \in \mathcal{S}_t^*(\mathbf{q}')} A_i(\mathbf{q}) + \Delta_{\text{att}}(\tau) \leq \tau^*(\mathbf{q}) + \Delta_{\text{att}}(\tau)$. By symmetry, also $\tau^*(\mathbf{q}) \leq \tau^*(\mathbf{q}') + \Delta_{\text{att}}(\tau)$. \square

Lemma 9 (Reuse lower bound). $\tau_{\text{pre}}(\mathbf{q}') \geq \tau_{\hat{S}_t}(\mathbf{q}) - \Delta_{\text{att}}(\tau)$.

Proof. $\tau_{\text{pre}}(\mathbf{q}') - \tau_{\hat{S}_t}(\mathbf{q}) = \sum_{j \in \hat{S}_t(\mathbf{q})} (A_j(\mathbf{q}') - A_j(\mathbf{q})) \geq -\|A(\mathbf{q}') - A(\mathbf{q})\|_1$. \square

b) *Covering drift with radius r :* Observation 2 and Theorem 6 imply that, along the sequence axis, cluster centers move by at most

$$\Delta_{\text{centroid}}(\tau) \leq 2(\text{diam } \mathcal{P}) \cdot \frac{K_{\max}}{\sqrt{d}} \sqrt{2-2\tau}.$$

Let $s(\tau)$ be any integer radius satisfying $s(\tau) \geq \Delta_{\text{centroid}}(\tau)$. If $r \geq s(\tau)$, $\mathcal{N}_r(\mathcal{S}_{t,m}(\mathbf{q}))$ covers the mean shift of the dominant modes between \mathbf{q} and \mathbf{q}' ; in particular, no additional loss is incurred from cluster translation outside $\hat{S}_t(\mathbf{q})$.

Proposition 2 (Pre-hoc retained-mass gap under CIS). *Assume $r \geq s(\tau)$ as above. Then*

$$\begin{aligned} \tau_{\text{pre}}(\mathbf{q}') &\geq \tau^*(\mathbf{q}') - 2\Delta_{\text{att}}(\tau), \\ \beta_{\text{th}}(\mathbf{q}') &\stackrel{\text{def}}{=} \tau^*(\mathbf{q}') - \tau_{\text{pre}}(\mathbf{q}') \leq 2\Delta_{\text{att}}(\tau). \end{aligned} \quad (42)$$

Consequently, with L candidate indices and baseline truncation $\delta^(\mathbf{q}')$ from TSA,*

$$\begin{aligned} I_{\text{full}}(\mathbf{q}') - I_{\text{pre}}(\mathbf{q}') &\leq 2[h_b(\delta^*(\mathbf{q}') + 2\Delta_{\text{att}}(\tau)) \\ &\quad + (\delta^*(\mathbf{q}') + 2\Delta_{\text{att}}(\tau)) \log L]. \end{aligned} \quad (43)$$

Proof. By Lemma 9, $\tau_{\text{pre}}(\mathbf{q}') \geq \tau_{\hat{S}_t}(\mathbf{q}) - \Delta_{\text{att}}(\tau)$. Since $\hat{S}_t(\mathbf{q})$ contains $\mathcal{S}_t^*(\mathbf{q})$ by definition, $\tau_{\hat{S}_t}(\mathbf{q}) \geq \tau^*(\mathbf{q})$. By Lemma 8, $\tau^*(\mathbf{q}) \geq \tau^*(\mathbf{q}') - \Delta_{\text{att}}(\tau)$. Combine to get $\tau_{\text{pre}}(\mathbf{q}') \geq \tau^*(\mathbf{q}') - 2\Delta_{\text{att}}(\tau)$. The MI bound follows by substituting $\beta_{\text{th}}(\mathbf{q}') \leq 2\Delta_{\text{att}}(\tau)$ into Eq. (4). \square

c) *When $r < s(\tau)$ (under-dilation):* Define the residual drift loss as

$$\varepsilon_{\text{drift}}(\mathbf{q}, \mathbf{q}'; m, r) \stackrel{\text{def}}{=} \sum_{j \in \mathcal{N}_{s(\tau)}(\mathcal{S}_{t,m}(\mathbf{q})) \setminus \mathcal{N}_r(\mathcal{S}_{t,m}(\mathbf{q}))} A_j(\mathbf{q}),$$

i.e., the attention mass (under \mathbf{q}) that can shift within $s(\tau)$ but lies outside the chosen radius r . Then the same proof yields

$$\beta_{\text{th}}(\mathbf{q}') \leq 2\Delta_{\text{att}}(\tau) + \varepsilon_{\text{drift}}(\mathbf{q}, \mathbf{q}'; m, r),$$

and the MI bound holds with β_{th} replaced by the PrHS. In practice we set $r = 1$ and increase m before r ; this covers the dominant modes while keeping $\varepsilon_{\text{drift}}$ negligible and the workload $\hat{S}_t \approx C_{\text{sink}} + C_{\text{local}} + k + m(2r)$ small.

B. Exponential Recency Beyond Sink

We adopt RoPE positional embeddings [43] and analyze their interaction with self-attention [21]. Excluding sink tokens, the multi-frequency rotations in RoPE cause phase dispersion with distance: representations of far-apart tokens become increasingly orthogonal in the rotated space, sharply reducing similarity (a *long-term decay* effect). Softmax attention amplifies this decay and translate it into exponentially smaller attention weights. Empirically, attention scores decrease roughly linearly or sublinearly with distance to the current token, while attention probabilities decay exponentially or faster, consistent with prior measurements [25, 26]. Thus, we assume there exist layer-dependent constants $\lambda_\ell > 0$ and a factor $\kappa_\ell \in (0, 1]$ such that for all $i > C_{\text{sink}}$,

$$A_i^{(\ell)}(\mathbf{q}_t^{(\ell)}) \leq \kappa_\ell (1 - \rho_\ell) \rho_\ell^{t-i}, \quad \rho_\ell \stackrel{\text{def}}{=} e^{-\lambda_\ell} \in (0, 1). \quad (44)$$

Equivalently, the non-sink portion of $A^{(\ell)}$ is dominated pointwise by a geometric tail with ratio ρ_ℓ and mass κ_ℓ .

In addition, the similarity of cross-layer hidden states (including keys and values) can exceed 95% beyond certain layer depth (generally with $\ell > N/2$) [34]. We then assume: for the per-layer key update $\Delta \mathbf{k}_i^{(\ell)} \stackrel{\text{def}}{=} \mathbf{k}_i^{(\ell)} - \mathbf{k}_i^{(\ell-1)}$, there exist $B > 0$ and $\mu > 0$ such that for the prefix to be frozen at layer ℓ ,

$$\max_{1 \leq i \leq E_\ell(t)} \|\Delta \mathbf{k}_i^{(\ell)}\| \leq B e^{-\mu(\ell-\ell_s)} \quad (45)$$

Lemma 10 (Logit change under key perturbations). *Let $a_i = \frac{1}{\sqrt{d}}(\mathbf{q}^\top \mathbf{k}_i)$ and $a'_i = \frac{1}{\sqrt{d}}(\mathbf{q}'^\top \mathbf{k}_i)$. Then*

$$\|a' - a\|_\infty \leq \frac{\|\mathbf{q}\|}{\sqrt{d}} \max_i \|\mathbf{k}'_i - \mathbf{k}_i\|.$$

Proof. Immediate from Cauchy–Schwarz.

C. PSAW Bounds on Dropped Mass

Following the PSAW selector defined in Sec. IV-B, and dropped set $\mathcal{D}_\ell = \{C_{\text{sink}} + 1, \dots, P_\ell(t) - 1\}$. The dropped mass at layer ℓ is $\delta_\ell^{\text{PSAW}} \stackrel{\text{def}}{=} \sum_{i \in \mathcal{D}_\ell} A_i^{(\ell)}(\mathbf{q}_t^{(\ell)})$. Let the window-start distance $D_\ell \stackrel{\text{def}}{=} t - P_\ell(t) + 1$ and satisfies $D_\ell \geq \lfloor u_\ell t \rfloor$.

Theorem 7 (PSAW worst-case bound). *Under (44), for every $\ell \geq \ell_s$,*

$$\delta_\ell^{\text{PSAW}} \leq (1 - \tau_{\text{sink}}^{(\ell)}) e^{-\lambda_\ell D_\ell} \leq e^{-\lambda_\ell D_\ell}.$$

Proof. Reindex non-sink positions by distance $d = t - i \in \{0, 1, 2, \dots\}$. Then \mathcal{D}_ℓ corresponds to $d \geq D_\ell$ and

$$\begin{aligned} \delta_\ell^{\text{PSAW}} &= \sum_{i \in \mathcal{D}_\ell} A_i^{(\ell)} \leq \kappa_\ell \sum_{d \geq D_\ell} (1 - \rho_\ell) \rho_\ell^d \\ &= \kappa_\ell \rho_\ell^{D_\ell} = \kappa_\ell e^{-\lambda_\ell D_\ell}. \end{aligned} \quad (46)$$

Since $\kappa_\ell \leq 1 - \tau_{\text{sink}}^{(\ell)} \leq 1$ the claim follows.

For the top layer $\ell = N$, $u_N = \phi^\alpha$ and $D_N \geq \lfloor \phi^\alpha t \rfloor$, we then have

$$\delta_N^{\text{PSAW}} \leq (1 - \tau_{\text{sink}}^{(N)}) e^{-\lambda_N \lfloor \phi^\alpha t \rfloor} \leq e^{-\lambda_N \phi^\alpha t}.$$

Given a target budget $\beta^{\text{PSAW}} \in (0, 1)$, any (ϕ, α) satisfying

$$\phi^\alpha \geq \frac{1}{\lambda_N t} \log \frac{1}{\beta^{\text{PSAW}} / (1 - \tau_{\text{sink}}^{(N)})}$$

ensures $\delta_N^{\text{PSAW}} \leq \beta^{\text{PSAW}}$. Otherwise, if $\lambda_\ell \geq \underline{\lambda} > 0$ almost surely and $\mathbb{E}[1 - \tau_{\text{sink}}^{(\ell)}] \leq 1$, then

$$\mathbb{E}[\delta_\ell^{\text{PSAW}}] \leq \mathbb{E}[(1 - \tau_{\text{sink}}^{(\ell)})] e^{-\lambda D_\ell} \leq e^{-\lambda D_\ell}.$$

D. ETF Bounds on Additional Mass Gap

For ETF define in Sec. IV-C, freezing means: for $i \leq E_\ell(t)$, set $\mathbf{k}_i^{(\ell)} \leftarrow \mathbf{k}_i^{(\ell-1)}$ and $\mathbf{v}_i^{(\ell)} \leftarrow \mathbf{v}_i^{(\ell-1)}$; for $i > E_\ell(t)$, compute as usual. Let $A^{(\ell)}$ denote the full (unfrozen) attention distribution and $\tilde{A}^{(\ell)}$ the distribution under ETF at layer ℓ . Define the ETF-induced mass gap (a total-variation budget)

$$\beta_\ell^{\text{ETF}}(\mathbf{q}_t^{(\ell)}) \stackrel{\text{def}}{=} \frac{1}{2} \|\tilde{A}^{(\ell)}(\mathbf{q}_t^{(\ell)}) - A^{(\ell)}(\mathbf{q}_t^{(\ell)})\|_1.$$

Theorem 8 (ETF: per-layer worst-case bound). *Following (45) and $\|\mathbf{q}_t^{(\ell)}\| \leq Q_{\max}$. Then*

$$\beta_\ell^{\text{ETF}}(\mathbf{q}_t^{(\ell)}) \leq \frac{Q_{\max}}{\sqrt{d}} B e^{-\mu(\ell-\ell_s)}.$$

Proof. Let $a_i = \frac{1}{\sqrt{d}}(\mathbf{q}_t^{(\ell)})^\top \mathbf{k}_i^{(\ell)}$ and $\tilde{a}_i = \frac{1}{\sqrt{d}}(\mathbf{q}_t^{(\ell)})^\top \tilde{\mathbf{k}}_i^{(\ell)}$, where $\tilde{\mathbf{k}}_i^{(\ell)} = \mathbf{k}_i^{(\ell-1)}$ if $i \leq E_\ell(t)$ and $\tilde{\mathbf{k}}_i^{(\ell)} = \mathbf{k}_i^{(\ell)}$ otherwise. Then $\Delta a_i = \tilde{a}_i - a_i = -\frac{1}{\sqrt{d}}(\mathbf{q}_t^{(\ell)})^\top \Delta \mathbf{k}_i^{(\ell)}$ for $i \leq E_\ell(t)$ and 0 otherwise. By Lemma 10 and (45),

$$\|\tilde{a} - a\|_\infty \leq \frac{\|\mathbf{q}_t^{(\ell)}\|}{\sqrt{d}} \max_{1 \leq i \leq E_\ell(t)} \|\Delta \mathbf{k}_i^{(\ell)}\| \leq \frac{Q_{\max}}{\sqrt{d}} B e^{-\mu(\ell-\ell_s)} \quad (47)$$

By Lemma 4, $\|\tilde{A}^{(\ell)} - A^{(\ell)}\|_1 \leq 2\|\tilde{a} - a\|_\infty$, hence $\|\tilde{A}^{(\ell)} - A^{(\ell)}\|_1 \leq 2 \frac{Q_{\max}}{\sqrt{d}} B e^{-\mu(\ell-\ell_s)}$. Divide by 2 to obtain the claim.

On the other hand, if $\mathbb{E}\|\mathbf{q}_t^{(\ell)}\| \leq \bar{Q}$, then

$$\mathbb{E}[\beta_\ell^{\text{ETF}}] \leq \frac{\bar{Q}}{\sqrt{d}} B e^{-\mu(\ell-\ell_s)}.$$

E. Joint pre-hoc retained-mass certificate and tuning

At layer ℓ , the overall pre-hoc mass budget from PSAW and ETF satisfies

$$\begin{aligned} \delta_\ell^{(\text{PSAW+ETF})} &\leq \underbrace{\delta_\ell^{\text{PSAW}}}_{\text{masking}} + \underbrace{\beta_\ell^{\text{ETF}}}_{\text{freezing perturbation}} \\ &\leq (1 - \tau_{\text{sink}}^{(\ell)}) e^{-\lambda_\ell D_\ell} + \frac{Q}{\sqrt{d}} B e^{-\mu(\ell-\ell_s)}, \end{aligned} \quad (48)$$

where $Q \in \{Q_{\max}, \bar{Q}\}$ depending on worst/average case. And at the top layer $\ell = N$, $\delta_N^{\text{PSAW+ETF}} \leq (1 - \tau_{\text{sink}}^{(N)}) e^{-\lambda_N \lfloor \phi^\alpha t \rfloor} + \frac{Q}{\sqrt{d}} B e^{-\mu(N-\ell_s)}$.

In practice, given targets $\beta^{\text{PSAW}}, \beta^{\text{ETF}} \in (0, 1)$, it suffices to choose (ϕ, α) and (ψ, γ) under average case such that

$$(1 - \tau_{\text{sink}}^{(N)}) e^{-\lambda_N \lfloor \phi^\alpha t \rfloor} \leq \beta^{\text{PSAW}}, \quad \frac{\bar{Q}}{\sqrt{d}} B e^{-\mu(N-\ell_s)} \leq \beta^{\text{ETF}}.$$

Equivalently,

$$\phi^\alpha \geq \frac{1}{\lambda_N t} \log \frac{1 - \tau_{\text{sink}}^{(N)}}{\beta^{\text{PSAW}}}, \quad N - \ell_s \geq \frac{1}{\mu} \log \frac{\bar{Q} B}{\beta^{\text{ETF}} \sqrt{d}}.$$